WATERAGRI

D6.2: Numerical Modelling Assessment

April 2023

WP6 Technical Evaluations

This project has received funding from the European Union's Horizon 2020 research and innovation programme under Grant Agreement No 858375.

Author(s)/Organisation(s)	Richard Hoffmann (FZJ), Harrie-Jan Hendricks-Franssen (FZJ), Philip Brunner (UNINE), Qi Tang (UNINE), Björn Klöve (OULU), Anna Autio (OULU), Wieslaw Fialkiewicz (UPWR), Arkadiusz Głogowski (UPWR), Attila Nagy (UNIDEB), Andrea Szabo (UNIDEB), Yu (Wayne) Wang (USAL)
Contributor(s)	Rolf Larsson (ULUND), Sebastian Puculek (ULUND)
Work Package	WP6
Delivery Date (DoA)	30/04/2023
Actual Delivery Date	30/04/2023
Abstract:	D6.2 "Model-based Assessments" shows the integration of selected WATERAGRI technologies in physically based models, such as irrigation scheduling and drainage control. The report documents the current status of near real-time modelling with physically based models developed at WATERAGRI case study sites in Finland, Poland, Hungary, Switzerland, and Germany. It demonstrates how improved irrigation scheduling and runoff/drainage management using physically based models can reduce the impacts of drought stress and overly wet conditions in the face of climate variability now and in the future.

Document Revision History			
Date	**Version**	**Author/Contributor/ Reviewer**	**Summary of main changes**
16/12/2022	V0	Richard Hoffmann (FZJ) – Editor	Template
07/03/2023	V1	Richard Hoffmann (FZJ) – Editor	Compiled version with input from all partners
04/04/2023	V2	Björn Klöve (OULU), Philip Brunner (UNINE) and Harrie-Jan Hendricks-Franssen (FZJ)	Review of V1
06/04/2023	V3	Richard Hoffmann (FZJ) – Editor	Revised draft after feedback from Reviewers
23/04/2023	V4	Richard Hoffmann (FZJ) – Editor	Final draft after revisions from partners
26/04/2023	V5	Sebastian Puculek (ULUND) – Contributor	Quality Control
26/04/2023	V6	Rolf Larsson (ULUND) – Contributor	Final Check
28/04/2023	VF	Richard Hoffmann (FZJ) – Editor	Final version

Dissemination Level		
PU	Public	**X**
CI	Classified information as referred to in Commission Decision 2001/844/EC	
CO	Confidential, only for members of the consortium (including the EC)	

WATERAGRI Consortium			
Participant Number	**Participant organisation name**	**Short name**	**Country**
1	LUNDS UNIVERSITET	ULUND	SE
2	EDEN MICROFLUIDICS	EDEN	FR
3	FORSCHUNGSZENTRUM JULICH GMBH	FZJ	DE
4	TEKNOLOGIAN TUTKIMUSKESKUS VTT Oy	VTT	FI
5	DEBRECENI EGYETEM	UNIDEB	HU
6	ALCHEMIA-NOVA GMBH	ALCN	AT
7	AGROGEO AGARFEJLESZTO-FOLDTANI-FOVALLALKOZO KORLATOLT FELELOSSEGU TATRSASAG	AGROGEO	HU
8	UNIVERSITAET FUER BODENKULTUR WIEN	BOKU	AT
9	ALMA MATER STUDIORUM UNIVERSITA DI BOLOGNA	UNIBO	IT
10	THE UNIVERSITY OF SALFORD	USAL	UK
11	COCONSORZIO DI BONIFICA DI SECONDO GRADO PER IL CANALE EMILIANO ROMAGNOLO CANALE GIANDOTTI	CER	IT
12	CENTRUM DORADZTWA ROLNICZEGO W BRWINOWIE	CDR	PL
13	INOSENS DOO NOVI SAD	INOSENS	RS
14	UNIWERSYTET PRZYRODNICZY WE WROCLAWIU	UPWr	PL
15	BAY ZOLTAN ALKALMAZOTT KUTATASI KOZHASZNU NONPROFIT KFT	BZN	HU
16	VULTUS AB	VULTUS	SE
17	TECHNISCHE UNIVERSITEIT DELFT	TU DELFT	NL
18	UNIVERSITE DE NEUCHATEL	UNINE	CH
19	AB GARDSTANGA NYGARD	GN	SE
20	OULUN YLIOPISTO	OULU	FI
21	AGRICOLUS SRL	AGRICOLUS	IT
22	INSTITUT NATIONAL DE RECHERCHE POUR L'AGRICULTURE, L'ALIMENTATION ET L'ENVIRONNEMENT	INRAE	FR
23	MARTIN REGELSBERGER	TBR	AT

Funding Scheme: Research and Innovation Action (RIA) ● Theme: SFS-23-2019
Start date of project: 01 May 2020 ● Duration: 48 months

Table of contents

List of figures

List of tables

1 General introduction

WATERAGRI is developing protocols to link observational data with models of hydrological, crop, land surface, vadose zone and subsurface processes in near-real time (WP2, WP7). Physically based models may allow better real-time management of water resources to quantitatively support agricultural decision-making in the face of a climate-related increase in extreme events and to improve water management in waterways such as canals. Task 6.2 in WP6 evaluates methods that potentially improve water retention in soil and contribute to improved irrigation and drainage. In this document, we present the evaluation of the impact and efficiency of the methods at the field scale and the scale of smaller agricultural watersheds, considering past and future weather variability in our physically based models, i.e., we present the current possible real-time modelling with our models.

It should be noted that some of the material presented and the description of WATERAGRI solutions is relevant to other work packages, e.g., D5.2, D6.1 (factsheets) and 7.5. Some descriptions of the codes, text, figures, and tables used may also be included in other work packages. Others, like the data assimilation framework, are only briefly described as this will be separately presented in D7.5.

2 Technical evaluation with physically based models

2.1 Assessment procedure

Fully distributed 3D integrated surface-subsurface hydrology (ISSHM) models are being developed for the case study sites in Germany, Switzerland, Hungary, Poland and Finland, covering different soils, crops and geologies. The models are designed to assess how improved irrigation planning, and runoff management can reduce the impact of drought stress and overly wet conditions in the face of increasing weather extremes (related to climate change) now and in the future. For example, this report will show how drainage systems can be optimized, when and how much to irrigate, and how to maintain ideal soil moisture conditions for different plant species with physically based models. We use either HydroGeoSphere (HGS) or the Terrestrial System Modeling Platform (TSMP) to simulate the water balance and/or the flow field of a given hydrogeological environment (details in D7.2).

HGS and TSMP allow joint simulation of surface water flow and water movement in the unsaturated zone (e.g., in the soil) and in the saturated zone (e.g., in an aquifer). The models consider spatially varying inputs such as precipitation, land use, plant species and subsurface hydraulic properties. We also consider site-specific soil, water, climate, and land use scenarios to develop accurate models of given agricultural conditions. The models are designed to provide the best possible forecasts of, e.g., soil moisture or groundwater levels. Thus, we are considering short-term weather forecasts, long climate change and different water and land use scenarios when we are using our models for forecasting. TSMP also simulates the water and energy exchange between land and atmosphere, the heat transport in the soil and vegetation development, and carbon and nitrogen fluxes and pools (e.g., nitrate leaching and nitrous oxide emissions). We choose TSMP for soil moisture simulation and assimilation and HGS for simulating and assimilating groundwater levels. TSMP is used for case study sites in Germany (Selhausen) and Hungary (Nyirbator) to mimic agricultural decision-making in the face of water scarcity in the first few meters of soil and, for example, to optimize irrigation schedules

with physically-based models. In contrast, HGS is selected for Finland, Poland, and Switzerland because of the focus on groundwater levels at the field and catchment scales, i.e., to mimic drainage system management and interactions with groundwater levels.

The development of a physically-based model is very time-consuming since the reality in the model should be discretized as best as possible, and the uncertainty of initial and boundary conditions, as well as of model parameters, must be quantified and minimized. Therefore, we are developing near real-time data assimilation in parallel for both modelling codes (see also below in D7.5) so that measurements from online sensor networks and the remote sensing pipeline can be used continuously for model calibration and prediction.

In general, work times of more than 400 h are quite typical for a reliable watershed model. Model run times typically range from a few minutes to a few hours, while very long spin-up runs or complex calibration procedures can significantly increase work and run times. However, the run time depends mainly on the machine and its available core-hours, the mesh resolution of the model (numerical grid), and the time step of the model input and output, as well as the required computation time step. For TSMP, the input data time step (e.g., of atmospheric forcings) is usually also the calculation time step. HGS can also be used with fixed time steps, but typically adaptive time steps are used when time varying boundary conditions are used.

2.2 Modelling codes

2.2.1 CLM/ParFlow

The Terrestrial System Modeling Platform (TSMP, Shrestha et al., 2014) combines compartmental models for the atmosphere (COSMO) (Baldauf et al., 2011), land surface (CLM 3.5; Oleson et al., 2008), and subsurface (ParFlow) (Ashby & Falgout, 1996; Kollet & Maxwell, 2006; Maxwell, 2013). For details on the convection-permitting atmospheric model COSMO, we refer to Baldauf et al. (2011) or Shrestha et al. (2014), as COSMO is not needed for the research questions of WATERAGRI. The land surface model CLM (Community Land Model) simulates the exchange of water, energy, carbon and nitrogen between the land surface and atmosphere, i.e., CLM calculates land-atmosphere fluxes, vegetation states, carbon and nitrogen pool dynamics, soil temperature and land surface temperature (Oleson et al., 2008). In CLM, plant physiological and crop parameters can be defined by specifying the percentage of a predefined plant functional type (pft) on the natural vegetation unit (% of area unit) and the percentage of a predefined crop functional type (cft) on the cropland unit for each grid cell. ParFlow calculates variably saturated groundwater flow by solving the Richards equation, and the calculation of surface water flow is based on the 1-D kinematic wave approximation of the shallow water flow equations. Equations are solved using a cell-centred finite difference scheme and implicit time integration (Ashby & Falgout, 1996; Kollet & Maxwell, 2006; Maxwell, 2013). When compartment models are coupled, information about fluxes and state variables is exchanged at the conceptual boundaries of the respective compartment models (Valcke, 2013; Gasper et al., 2014; Shrestha et al., 2014). For example, CLM calculates net infiltration, provided to ParFlow, which calculates pressure in the unsaturated zones and overland flow. So, ParFlow provides pressure and soil moisture contents to CLM, which uses this in various calculations, for example, for ET, i.e., the hydrology of CLM is replaced with the hydrology of ParFlow (Kurtz et al., 2016). The modular character of TSMP also allows the

compartment models to operate independently of each other or to use only two neighbour compartment models (e.g., CLM-ParFlow or CLM-COSMO).

It should be noted that CLM 3.5 in TSMP is being updated to CLM5, which has some fundamental improvements over version 3.5. The new features allow for more realistic, site-specific simulations to meet the goals of WATERAGRI, i.e., the needs of stakeholders consulted in workshop #3 (we refer to Lawrence et al. (2019) for details on CLM 5). For example, in CLM5, soil evaporation is now controlled by the diffusion rate of water vapour through a dry surface layer (Kennedy et al., 2019; Lawrence et al., 2019; Swenson et al., 2019). CLM5 accounts for soil layers of varying thicknesses, as well as 20 hydraulically active and 5 hydraulically inactive layers, i.e., an underlying impermeable bedrock or zero-flow soil boundary condition. Therefore, CLM5 can now explicitly simulate saturated and unsaturated zones and the associated groundwater level (Lawrence et al., 2019). The accuracy and stability of the numerical soil water solution in CLM5 have been improved by introducing an adaptive time-stepping solution to Richard's equation (Lawrence et al., 2019). CLM5 can calculate the vegetation states prognostically now and has increased the number of plant functional types and crop functional types, which allows a more fine-grained representation of the different vegetation types and the yearly cycles of vegetation states (Kennedy et al., 2019; Lawrence et al., 2019; Swenson et al., 2019; Boas et al., 2021). As a result, CLM5 standalone can provide robust site-specific information on decision-critical parameters, e.g., soil water content, leaf area index and crop biomass, which, compared to CLM3.5, are expected to be more reliable, given the implemented model improvements. Compared to CLM3.5-ParFlow, a major advantage is that less compute time is needed and less time has to be spent on model setups.

2.2.2 HydroGeoSphere

(The text below is largely identical to the text of the HydroGeoSphere model code description in Deliverables D3.1 and D7.2)

HydroGeoSphere (HGS) (Brunner & Simmons, 2012; Schilling et al., 2019; Aquanty, 2020) is a physically based and fully distributed integrated hydrological model that has been successfully applied in many different hydrogeological contexts and at many different spatial and temporal scales. HGS can explicitly simulate the interactions between groundwater, surface water and vegetation considering variably saturated subsurface flow and complex heterogeneous subsurface properties (e.g., Schilling et al., 2014; Ala-aho et al., 2017; Schilling et al., 2017; Tang et al., 2018). HGS can also consider fully explicit contaminant or nutrient transport and irrigation and tile drainage in agricultural contexts (e.g., Bonton et al., 2012; Schepper et al., 2017). HGS has been coupled to the Weather Research and Forecast (WRF) model for the integrated simulation of the atmosphere, surface, and subsurface interactions (Davison et al., 2015) and has been used for data assimilation experiments using the ensemble Kalman filter (EnKF) (Kurtz et al., 2017; Tang et al., 2017; Tang et al., 2018).

In HGS, the surface and subsurface are represented by two domains, the overland domain and the porous medium domain. Surface water flow, i.e., flow within the overland domain, is represented with the following diffusion-wave approximation of the two-dimensional Saint-Venant equation:

$$\frac{\partial \varphi_o h_o}{\partial t} = -\overline{\nabla} \cdot d_o \mathbf{q}_o - d_o \Gamma_{ex} \pm Q_o$$

Where $\overline{\nabla}$ is the two-dimensional differential operator, d_o [m] is the depth of surface water (excluding rill storage height that represents microtopography), φ_o [-] is the surface flow equivalent porosity that accounts for microtopography, h_o [m] is the total head ($\equiv z + d_o$) for given water depth d_o and elevation z, $\mathbf{q}_o$ [m/d] is the average surface water flow velocity, Γ_{ex} [m/d] is the volumetric rate of fluid exchange between the surface and subsurface domains per unit surface area (positive when water flows from the surface to the subsurface), and Q_o [(m^3/d)/m^3] represents sources and sinks (volumetric flux per unit surface area). The surface flow equivalent porosity ranges between 0 and 1, depending on whether the depth of surface water is below or above the microtopography.

The average surface water flow velocity $\mathbf{q}_o$ is given by:

$$\mathbf{q}_o = -\mathbf{K}_o \cdot k_{ro} \nabla(h_o)$$

where k_{ro} is a dimensionless factor accounting for obstructed flow and microtopography, and $\mathbf{K}_o$ [m/d] is the surface conductance that is solved using Manning's equation.

Irrigation is simulated in HGS by aligning the numerical grid during mesh generation with irrigation infrastructure, e.g., drip irrigation piping, and by subsequently specifying representative irrigation water fluxes [m^3/d] via second-type (Neumann) boundary conditions at discrete model nodes located within the surface domain.

Variably-saturated groundwater flow in HGS is simulated using Richards' equation:

$$\frac{\partial}{\partial t}(\theta_s S_w) = -\nabla \cdot \mathbf{q} + \Gamma_{ex} \pm Q_o$$

where θ_s [-] is the saturated water content, S_w [-] is the water saturation, $\mathbf{q}$ [m/d] is the groundwater flux (i.e. Darcy flux), and Q_o [(m^3/d)/m^3] represents sinks and sources (volumetric flux per unit volume).

The groundwater flux $\mathbf{q}$ is given by:

$$\mathbf{q} = -k_r(S_w)\mathbf{K} \cdot \nabla(\psi_w + z)$$

where $k_r(S_w)$ [-] is the relative permeability of the medium, $\mathbf{K}$ [m/d] is the saturated hydraulic conductivity tensor of the porous medium, and ψ_w and z [m] are the pressure and the elevation head, respectively. Surface water flow and groundwater flow equations (i.e., the overland and the porous medium domains) are fully-coupled with the dual-node approach (Rooij, 2017) and are solved simultaneously, without requiring iteration. The relationship between the relative permeability of the porous medium, the soil water content and pressure, can be given in tabular form or can be parametrized using the Van Genuchten functions (van Genuchten, 1980).

According to the approach of (van Genuchten, 1980), the saturation S_w is related to the matric suction ψ and the relative permeability k_r by:

$$S_w = \begin{cases} S_{wr} + (1 - S_{wr})\left[1 + |\alpha\psi|^{\beta}\right]^{-\upsilon}, & \psi < 0 \\ 1, & \psi \geq 0 \end{cases}$$

$$k_r(\psi) = {S_e}^{(l_p)}\left[1 - \left(1 - {S_e}^{1/\upsilon}\right)^{\upsilon}\right]^2$$

$$S_e = (S_w - S_{wr})/(1 - S_{wr})$$

where S_{wr} [-] is the residual saturation, α [L^{-1}] and υ [-] are the van Genuchten parameters, υ is given as $1 - {}^{1}/_{\beta}$ with $\beta > 1$, S_e [-] is the effective saturation and l_p [-] is the pore-connectivity parameter (which is 0.5 for the van Genuchten model).

Evapotranspiration is modelled as a combination of evaporation and transpiration, affecting both the surface and the subsurface. Transpiration T_p [LT^{-1}] is simulated based on the implementation of (Kristensen & Jensen, 1975)

$$T_p = f_1(LAI)\, f_2(\theta)\, RDF\, [E_{pot} - E_{canopy}]$$

$$f_1(LAI) = \max\{0, \min[1, (C_2 + C_1 LAI)]\}$$

where *LAI* [-] is the leaf area index, θ [-] the soil moisture content, *RDF* [-] the root decay function, E_{pot} [LT^{-1}] the potential evapotranspiration, E_{canopy} [LT^{-1}] interception and canopy evaporation, and C_1 [-] and C_2 [-] are coefficients which express the relation of transpiration on LAI. C_1 allows accounting for transpiration limiting vegetation characteristics (e.g., height, development stage, age of vegetation, degradation) and C_2 for transpiration from vegetation for which LAI can't be defined. The *RDF* describes the decrease of root density with depth. $f_2(\theta)$ takes on values between zero and one according to:

$$f_2(\theta) = \begin{cases} 0, & 0 \le \theta \le \theta_{wp} \\ f_3, & \theta_{wp} \le \theta \le \theta_{fc} \\ 1, & \theta_{fc} \le \theta \le \theta_{ox} \\ f_4, & \theta_{ox} \le \theta \le \theta_{an} \\ 0, & \theta_{an} \le \theta \end{cases}$$

$$f_3 = 1 - \left[\frac{\theta_{fc} - \theta}{\theta_{fc} - \theta_{wp}}\right]^{C_3}$$

$$f_4 = 1 - \left[\frac{\theta_{an} - \theta}{\theta_{an} - \theta_{ox}}\right]^{C_3}$$

Below the wilting point θ_{wp} [-], transpiration is zero, maximum transpiration is reached between the field capacity θ_{fc} [-] and the oxic limit θ_{ox} [-], and if the soil moisture content is above the anoxic limit θ_{an} [-], root stress is so high that transpiration is again 0 (Feddes et al., 2004). C_3 [-] is a fitting parameter with a recommended value of 1, making the ramping functions f_3 and f_4 linear (Feddes et al., 1978; Panday & Huyakorn, 2004).

Agricultural drainage infrastructure such as tile drains could be efficiently simulated in HGS using so-called 1-D pipe elements, which circumvents the computationally intensive calculations that would be necessary if drainage flow were considered explicitly as part of the variably saturated subsurface porous medium flow domain. Instead, drainage flow in tile drains is simulated using the efficient one-dimensional Hazen-Williams equation (Aquanty, 2020). This, however, requires that the numerical grid is aligned with drainage infrastructure already during mesh generation, such that the specification of the 1-D drainage network is possible via discrete model node selections.

3 WATERAGRI solutions

3.1 Drainage systems

Real-time assessment of different options (e.g., closing certain drains in times of drought) to operate the drains is implemented in the integrated physically based models combined with data assimilation (A2). The real-time active drainage control will enable precise irrigation schemes considering surface and subsurface water resources. Moreover, the efficiency of costly investments such as new drainage systems or irrigation systems is assessed under consideration of climate change. The real-time modelling and active drainage management form part of the framework (A1) developed in WP7 (see also later D7.5).

3.2 Irrigation systems

Irrigation is usually the first measure to protect sensitive crops from prolonged droughts. However, irrigation is water intensive and can alter groundwater recharge, negatively impacting groundwater quality in irrigated areas (Pulido-Bosch et al., 2018). Therefore, WATERAGRI is developing an online platform to provide the best possible estimates of irrigation needs for selected agricultural plots. Hourly weather data, soil properties, remote sensing information, crop development stage, irrigation amounts provided by farmers, and weather forecasts are input data for soil water balance calculations and numerical simulations designed to add on precision irrigation. We evaluate the reliability of integrated models that predict plant-critical soil moisture conditions days in advance and estimate the amount of water that needs to be restored to the soil.

3.3 Data Assimilation Framework

Uncertain initial and boundary conditions, as well as input parameters and their spatial distribution, can limit the reliability of numerical models. Within WATERAGRI, data assimilation techniques are used in addition to classical calibration methods to quantify and reduce model uncertainties. Data assimilation protocols will be developed in Germany and Switzerland. In Finland and Poland, we use first a calibration procedure. Later we will perform data assimilation on all sites. TSMP, just like CLMv5, is coupled with the generic data assimilation library "Parallel Data Assimilation Framework" (PDAF) for this purpose (Nerger & Hiller, 2013; Kurtz et al., 2016; Strebel et al., 2022). TSMP-PDAF or CLMv5-PDAF allows correcting model simulations with measurements to constrain initial conditions and parameters. We use the ensemble Kalman filter, which is a sequential method where nonlinear dynamical systems are stochastically approximated using Monte Carlo methods (Burgers et al., 1998; Reichle, 2008). Here, an ensemble of model runs, which approximate the model uncertainty, is run and used to estimate the model error covariance matrix, which is essential in the data assimilation procedure to weigh, on the one hand, the model predictions and, on the other hand, the measurements. Deviations between measurements and model predictions are used to update the model predictions, and the correcting influence of the measurements depends on the relative weights assigned to the model prediction and measurements, as calculated by the data assimilation algorithm.

3.4 Water retainer

WATERAGRI develops an enhanced water retention concept. The Water Retainer is an organic soil conditioner liquid that can be added to the soil. It is designed to help plants better taking-up water and to reduce evaporation from bare soil. Ultimately, the water retainer changes the physical properties of the soil/shallow subsurface, which can be considered in numerical simulations, i.e., in the parameterization. This change is intended to result in improved drought resistance, which should then reduce the effects of drought and dehydration.

4 Model-based Assessment

4.1 Finland-Tyrnävä (T5.1): Optimization of irrigation and drainage control (HGS)

4.1.1 Brief site description

The Tyrnävä field (6.4 ha) is located in the municipality of Tyrnävä in the Northern Ostrobothnia region, Finland (Figure 1) within the Temmesjoki watershed. The Tyrnävä region has a long agricultural history, and the region is known for its production of potatoes and is a key seed potato region in Europe. The Tyrnävä site is currently used for industrial potato production, which are typically relatively late yield collection times (usu. late September) to increase the potato's starch content. The field is surrounded by open ditches connected to the vast network of open drainage covering the whole sub-catchment. The field is tile drained, and the drainage system was renewed in the autumn of 2017.

The region is characterized by a boreal climate with an average annual temperature of 3.4 °C and precipitation of 582 mm for the years 2000-2020 (derived from daily 1 km x 1 km gridded time series (Aalto et al., 2016). The average annual reference evapotranspiration for 2015-2020 was around 480 mm (derived from daily 1 km x 1 km gridded reference evapotranspiration time series estimated by FAO Penman–Monteith method; Pirinen et al., 2022).

The Tyrnävä field is located within the Muhos formation and is characterized by thick unconsolidated sediments extending up to 100 m depth (Geological Survey of Finland, 2017). The top soils in the Tyrnävä region consist predominantly of fines: fine sand with silt and clay layers. These fine-graded sediments are outwash materials accumulated during and after the last deglaciation period from the higher elevated areas by the glaciofluvial, aeolian and littoral processes and have thicknesses up to 20 m (Johansson et al., 2005). The deeper sediments are more permeable sand deposits. The site's terrain is low-laying plain with minor topographic relief that explains the little occurrence of peatlands. Peat soils are usually relatively thin (less 1 m, Johansson et al. (2005). The field soil was classified as "löyhä karkea hieta" (Liedes et al., 2020) that it a term that refers to loose fine sands or coarse silts.

Field hydrogeological monitoring includes water level in shallow groundwater pipes (AA1-AA3 and AV1-AV3 for years 2018-2019, GWp1-GWp4 for years 2022-2023), water level observations in tile drainage control wells (AA and AV for 2018-2019 and 2021), and soil moisture observations (AA1-AA3, AV1-AV3 for years 2019 and AA and AV for years 2021-2023).

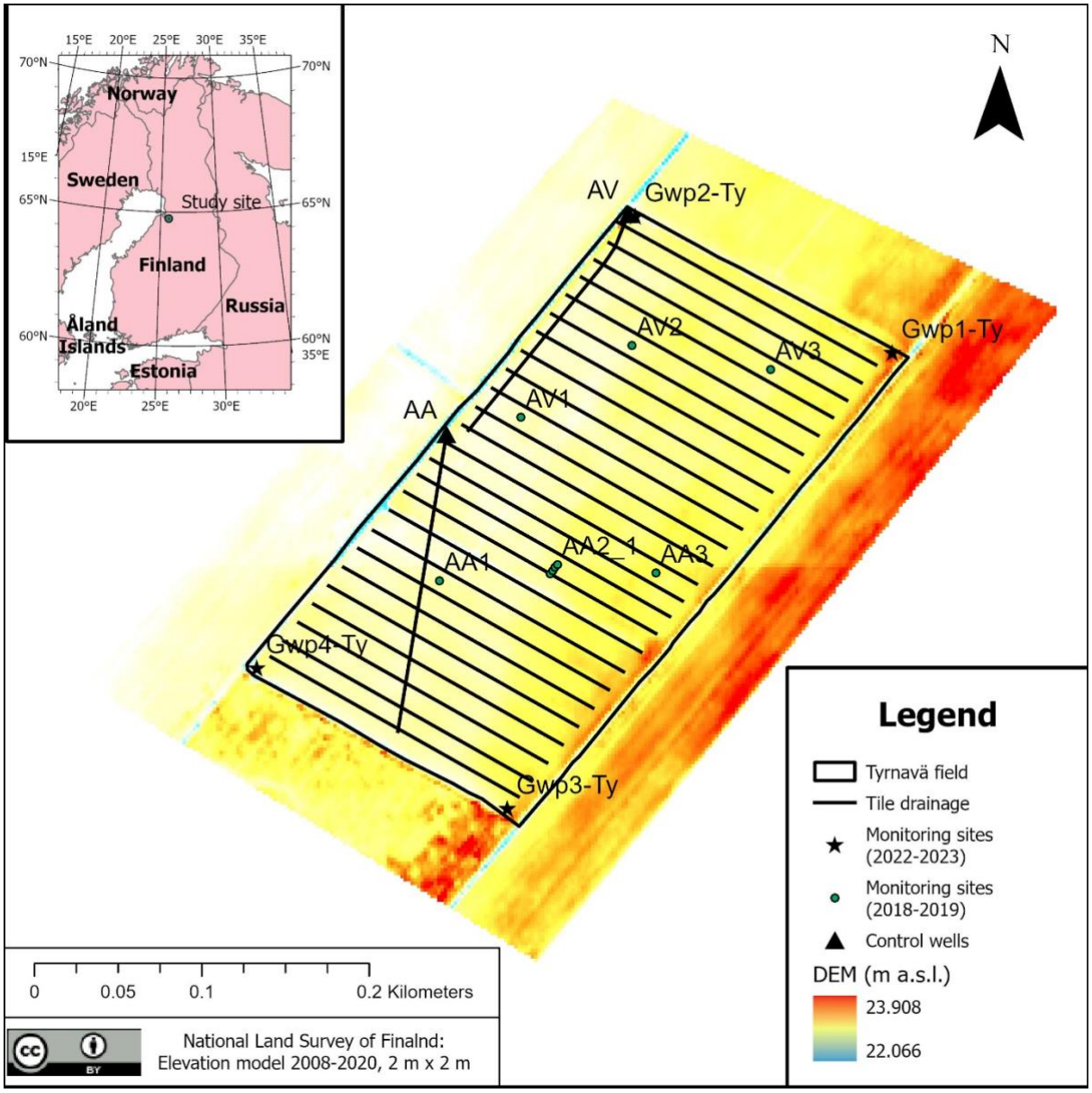

Figure 1. The Tyrnävä potato field study site with monitoring locations and tile drainage network. The land surface elevation (DEM) used to define the model boundaries is presented in the background.

Currently applied water management agricultural practices

The main aim of the water management activities for potato production is to accelerate the drying of the field during wet times in order to achieve sufficient load-carrying capacity for other agricultural operations and create optimal conditions for crop cultivation. The drainage can usually be achieved through open ditch networks, traditional tile drainage systems, or controlled drainage systems. From these, only the controlled drainage systems allow for groundwater level regulation within the field area and, more importantly, soil moisture control.

In control drainage systems, the farmer adjusts the water table elevation through the control well structure (Figure 5 in D5.2) to optimize soil moisture conditions for a given crop production. This is especially beneficial for moisture-sensitive soil types of crops. For instance, potato crops are sensitive

to moisture content at certain times of growth. Both wet and dry conditions limit production. The wet conditions cause plant drowning and, in extreme cases, die-offs but also favour the spread of diseases (Fiers et al., 2012).

In contrast, too-dry conditions were found to directly correlate with the size of potatoes and the final yield (e.g., Martin et al., 1992). The drainage control should also allow heavy agricultural machinery for the required work. Also, potato is a high-value crop to which control systems can be cost-efficient.

The Finnish Rural Network Support Unit (Maaseutunverkosto, 2009) recommends the following general management of control drainage: The check gate of the control well is open throughout the spring season and closed as soon as the field dries enough, and the load-carrying capacity of the soil is sufficient for agricultural machinery. After that, the check gate is closed and adjusted to the target height. The gate is opened a sufficient time before harvesting to ensure good soil load-carrying capacity**.** After the harvesting and autumn ploughing, the check gate should be closed again to rewet the soil and decrease nutrient loss. It is recommended to keep the gate open during the winter season to avoid the tile drainage system freezing, but in case of mild winters, the system might remain closed. In case of forecasted heavy rains, the gate should be opened to avoid field inundation. In practice, the activity of farmers to control tile drainage systems varies, and some farmers more actively adjust the control wells during summer times, but usu. this is not done very often for logistical reasons; adjusting manual valves in multiple fields is time-consuming.

4.1.2 Model/Method description

The focus of the WP 6.2 was to evaluate how the different technical solutions for retention/irrigation can be simulated with mathematical models.

This study is conducted in the form of modelling scenarios testing various control drainage practices, including use as an irrigation system. The scenarios tested and planned for the Tyrnävä model are listed in Table 1. The calibrated model of Case D2 will be further developed for testing management scenarios case M1-2 and used in the data assimilation experiment D7.5.

Modeling scenarios enable the development of realistic predictions of how various water management practices work to sustain optimal potato growth conditions in the Tyrnävä region. In the scenario modelling approach, a base case model is implemented, and the impact of various water management practices is tested by changing parameter sets/inputs and/or implementing features related to the evaluated aspect. For instance, the base case can represent a system with no tile drainage, i.e., a situation before the new tile drainage system at the field site was built. One of the evaluated solutions could be using a traditional tile drainage system, i.e., the tile drainage without a control well. For this scenario, a new model version is built with implemented tile drainage network and model required model boundary conditions and parametrization for such structures. The outputs of the new model version than can be compared to the base case and the impact of the traditional tile drainage system on the water conditions in the field can be inferred.

Table 1. Modeling scenarios to test various water management in control drainage systems. For each case, an aspect modified is mentioned.

Scenario	Description	Objective	State
Base case (BC)	Field site model with no drainage network implemented and no-flow BC		conducted
Case BC1	Natural gradient constant head conditions are derived from DEM 2m x 2m product	Evaluation of the impact of boundary conditions on the model outputs	conducted
Case D1	Drainage network implemented; control structures not used	Assessment of a tile drainage system on water conditions	conducted
Case D2	Drainage network implemented; control structures used (current management practice)	Assessment of a control tile drainage system on water conditions	conducted
Manual model calibration			
Case M1	Use of arbitrary source of water for irrigation	To test if the tile drainage system can be successfully utilized as an irrigation system to mitigate drought impacts on potato production	planned
(Case M1a)	Use of irrigation pond water for irrigation during drought periods, water supplied by the tile drainage network	This scenario will be tested if the solution of the scenario M1 is feasible; To evaluate various water sources for the irrigation	planned
(Case M1b)	Use of deep groundwater during drought periods, water supplied by the tile drainage network (requires the use of more extensive modelling domain)	This scenario will be tested if the solution of the scenario M1 is feasible; To evaluate various water sources for the irrigation	planned
Case M2	Active tile drainage control: adjustable water level in the tile drainage control structure according to moisture conditions	To test how control drainage schedule can be optimized to provide optimal conditions for potato production	planned
Data assimilation + M1-M2 (D7.5)			

Modelling objectives

The main objectives of the field-scale modelling exercise with the HGS are: (i) to evaluate the effectiveness of the current drainage management; (ii) to evaluate different drainage control practices and use tile drainage network as an irrigation system for droughts mitigation using, for example,, stream/open ditch water or deep groundwater; (iii) real-time assessment of different water management options, for instance, closing control tile wells in case of probable drought on the base of the meteorological forecasts, (iv) study surface and groundwater interactions in the field-scale.

Base case model implementation in HGS

The base case model domain was limited to the area between the deepest parts open ditch surrounding the Tyrnävä field and was delineated using the 2m x 2m digital elevation model (DEM; National Land Survey of Finland, 2023). The two-dimensional triangular mesh was built in AlgoMesh v 2.0.19.19384, consisting of 3102 elements and 3102 nodes. The grid nodes coincide with the location of monitoring sites and the tile drainage network (Figure 2).

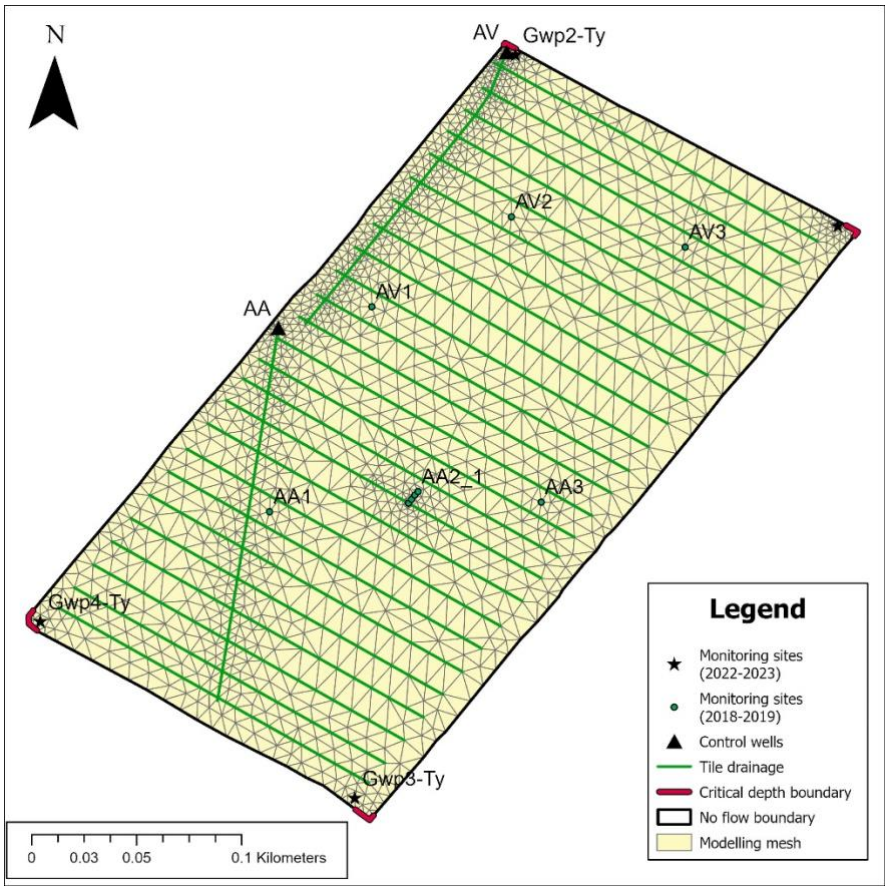

Figure 2. Two-dimensional triangular mesh for the Tyrnävä potato field model with monitoring network and implemented control tile drainage system.

The model domain conceptualization was based on the generic agricultural soil profile for the region, shallow and deep drillings (Geological Survey of Finland, 2017), and field observations. The modelled soil profile was divided into five major soil zones typical for the Tyrnävä region: relatively permeable furrow zone, less permeable subsoil, tightly compacted undersoil ("jankko"), deep subsoil, and sandy

soil of the Muhos formation (Figure 3). The fine-graded soil properties were derived from literature except for the pF properties collected during sensor installation for the top soil layers and measured in the laboratory with the pressure plate apparatus (Figure 4). The sand layer properties are the default HGS values for sand. The soil water characteristics were represented in the model by Mualem-van Genuchten functions derived from the measured data. Figure 4Due to uncertainty in bedrock depth, the bedrock layer was assumed to be represented by a flat surface located approximately 50 m below the land surface (the area has one of the deepest soils in Finland). More details on the soil profile conceptualization are presented in Table 2, and the parameter values used in the base model are in Table 3. The surface topography of the model domain is based on 2 m x 2 x DEM (National Land Survey of Finland, 2023) modified to incorporate open ditches at the model domain perimeter.

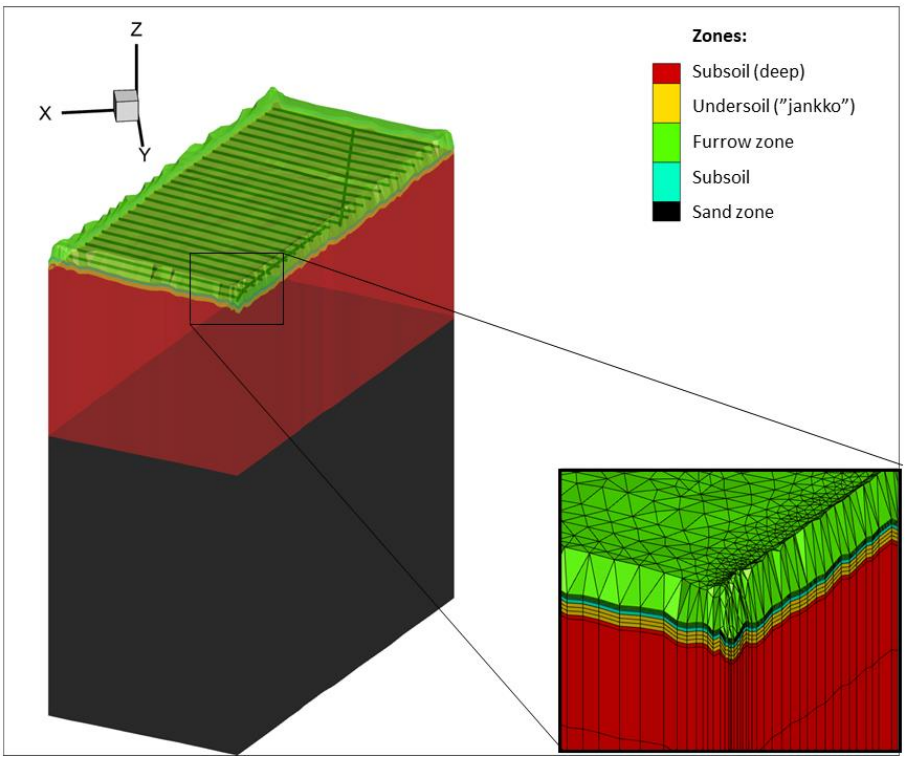

Figure 3. Three-dimensional view of the model domain with various coloring for main soil layers. The vertical exaggeration is ten times the horizontal.

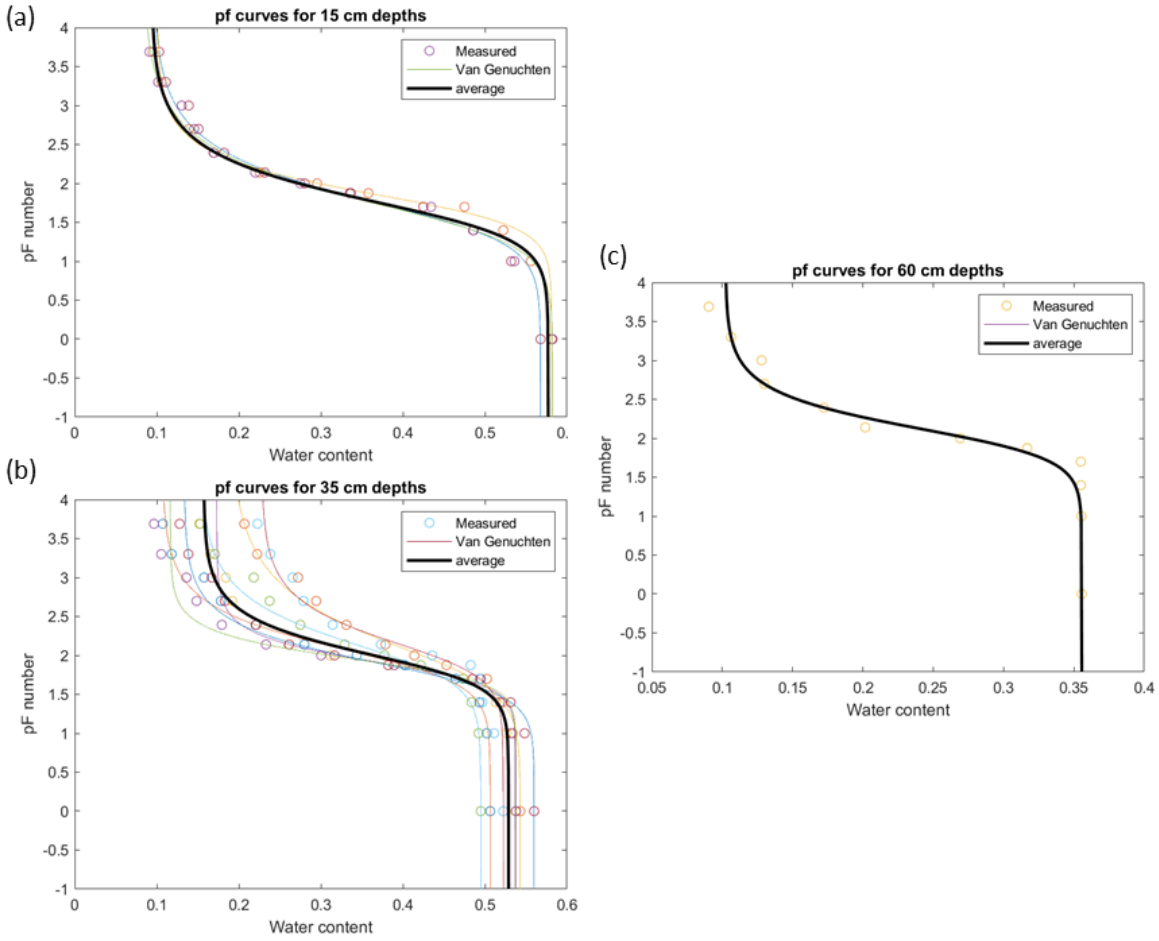

Figure 4. pF-curves measured at (a) 15 cm, (b) 35 cm and (c) 60 cm depth, using the pressure plate apparatus and fitted Van Genuchten water retention curves. Each color represents a different sample.

Table 2. Conceptualization of soil layer profile of the Tyrnävä potato field model.

Layer name	Layer thickness (m)	Depth of the layer's top from the land surface (m)	Hydraulic conductivity (m/s)/ Anisotropy ratio (Kxy/Kz)	Comments
Furrow zone	0.15	0	$8.0x10^{-6}$ / 2	Represents furrow layer of approximately 30 cm thickness; pF properties measured
Subsoil	0.20	-0.15	$4.0x10^{-6}$ / 2	pF properties measured
Undersoil ("Jankko")	approximately 0.40-0.80	-0.35	4.0×10^{-7} / 2	Variable thickness layer; poorly conductive zone compacted by the heavy agricultural machinery; pF properties measured
Subsoil (deep)	approximately 19	approximately -0.75-1.2 m	$4.0x10^{-6}$ / 2	Variable thickness layer; no data but assumption is that it is more permeable than undersoil; pF properties assigned to be same as for undersoil
sand zone	30	20	7.438×10^{-5}	The properties of this layer cannot be verified from the current monitoring setup; default HGS values for sand
Bedrock	-	50	-	Bottom of the modelling domain

Table 3. Soil hydraulic parameters used in the simulation.

Parameter\Zone	Furrow zone	Subsoil	Undersoil ("Jankko	Subsoil (deep)	Sand zone
Subsurface					
Kxy (m/s)	8.0E-06 [a]	4.0E-06 [a]	4.0E-07 [b]	4.0E-06 [a]	7.4E-05 [d]
Anisotropy ratio Kxy/Kz	2 [b]	2 [b]	2 [b]	2 [b]	1 [d]
Specific storage (1/m)	1.0E-03 [b]	1.0E-03 [b]	1.0E-03 [b]	1.0E-03 [b]	1.0E-04 [d]
Porosity	0.58 [c]	0.53 [c]	0.36 [c]	0.36 [b]	0.375 [d]
Residual saturaton S_r	0.16 [c]	0.3 [c]	0.29 [c]	0.3 [b]	Unsaturated flow relation type Pseudo-soil [d]
van Genuchten alfa (1/m)	2.56 [c]	1.29 [c]	0.97 [c]	1.29 [b]	Unsaturated flow relation type Pseudo-soil [d]
van Genuchten beta	1.98 [c]	2.32 [c]	2.4 [c]	2.32 [b]	Unsaturated flow relation type Pseudo-soil [d]
Minimum relative permeability (m/s) [1]	1.0E-02 [b]	1.0E-02 [b]	1.0E-02 [b]	1.0E-02 [b]	Unsaturated flow relation type Pseudo-soil [d]

Sources: [a] Rintanen, 1985; [b] professional judgment; [c] measured; [d] HGS default

The potato field farrow topography in the current setup of the model was not directly implemented but represented as a uniform soil layer of 15 cm thickness. The overland domain properties and actual evapotranspiration properties are represented by uniform zones for the whole domain and are based on the literature review and professional judgment. The overland and evapotranspiration parameter values used in the base case model are shown in Table 4 and Table 5.

Table 4. Overland flow properties used in the simulations.

Parameter\Zone	Potato Field	Source/Rationale
Manning's n ($s/m^{1/3}$)	0.04	(Chow, 1959)
Rill storage height (m)	0.05	Professional judgment
Obstruction storage height (m)	1.0E-03	For simplification not included
Coupling length	1.0E-03	Liggett et al., 2012

Table 5. Evapotranspiration parameters used in the simulations.

Parameter\Zone	Potato field	Rationale
Interception parameters		
Canopy storage parameter (m)	0	For simplification not included
Initial interception storage (m)	0	For simplification not included
Transpiration fitting parameters		
C1	0.5	Default
C2	0	Default
C3	1	Default
Transpiration limiting pressure head		
Wilting point (m)	-150	Typical suction pressure to define wilting point
Field capacity (m)	-3.3	Typical suction pressure to define field capacity
Oxic limit (m)	0	Potatoes cannot tolerate waterlogged conditions
Anoxic limit (m)	0	Potatoes cannot tolerate waterlogged conditions
Evaporation limiting pressure head		
Minimum (m)	-1.5	Professional judgment
Maximum (m)	-0.42	Professional judgment
Others		
Leaf area index LAI	1.5	Potato of LAI varies during the year and varies significantly from crop to crop
Root zone depth (m)	0.35	Potatoes roots are unable to grow in the subsoil
Root profile RDF	Rdf quadratic decay function	
Evaporation depth (m)	0.2	Default
Evaporation profile	Edf quadratic decay function	

The perimeter and the bottom of the subsurface domain (impermeable bedrock) were prescribed no-flow boundaries. For the overland domain, we used critical depth boundary conditions at each model domain corner. Such implementation allows water to freely leave the model domain at each ditch outlet (Figure 2) as, according to our observations, the flow direction in the field open ditch system is poorly defined. Otherwise, no flow boundary conditions were prescribed on the borders of the overland flow domain.

The current model was run in a transient state between 1st January 2015 and 31st December 2020. First, the steady-state model was solved by forcing the model with typical for the Tyrnävä region's effective rainfall (annual precipitation subtracted annual reference evapotranspiration) equal to approximately 300 mm/year. Then, the attained steady-state model solution was used as the initial conditions for the transient-state runs. The transient runs were forced by 1km x 1km gridded precipitation, temperature (Aalto et al., 2016), and reference evapotranspiration (Pirinen et al., 2022) time series at daily timesteps. Future model runs will extend the simulation period to cover the years 2021-2023. All Tyrnävä field simulations were run with HGS (version 2482) in the finite difference mode and used the dual approach for surface and subsurface coupling.

The tile drainage network was implemented into the HGS model using the slope and pipe height information derived from tile drainage plans conducted by Maveplan Oy, a private sector company specializing in geotechnical investigation and structural engineering. The view of the model mesh with implemented drainage network is shown in Figure 2. The 'Simple drain' boundary condition enabled water outflow from the tile drainage system. The control tile drainage was adjusted according to the following scheduling scenario: the control tile drainage was open for spring periods 1.4.2018-22.4.2018, 1.4.2019-14.5.2019 and 1.4.2020-14.5.2020, and otherwise kept closed.

4.1.3 First results

First, we present the simulation results: the base model and modelling scenario BC1 testing applied boundary conditions and scenarios D1-D2 presenting the impact of tile drainage and control tile drainage systems. Furthermore, in the section "Lessons learned and future model development, " we discuss what we learned from the current results, how this knowledge should be used in further model development, and propose a possible calibration procedure to be implemented.

The measured and transient-state groundwater levels for each modelling scenario are presented in Figure 5 and Figure 6. The limited measurement period durations allow only tentative evaluation of the model performance. The base case model with no tile drainage system well captured the general trends and magnitudes of measured groundwater levels but missed the dynamic and steep hydrograph rises and recession caused by strong rainfall events. The base case simulation shows that with no tile drainage system, the field can be temporarily fully saturated with the water table being at the land surface during wet seasons (autumn/spring) but with overall shallow water tables (less than 1 m below land surface) also during wet summers.

In order to test the impact of the assigned boundary conditions, we run the model with constant regional specified head boundary conditions (BC1). Figure 5 and Figure 6 show that under such boundary conditions, the model field behaves differently than in the base case scenario; the groundwater levels are overall less variable, with a higher water table for the summers and lower water levels for the winter periods. The flattening impact of the boundary conditions is visible relatively far from the model boundary (e.g., AV1 and AA3), also in the locations in the middle of the field (AA2 and AV2), indicating that the current model is susceptible to the prescribed boundary conditions.

The tile drainage scenario D1 shows the apparent beneficial effect of the tile drainage system. After constructing the tile drainage system, the field reaches new drier conditions leading to relatively stable water levels within 2-3 weeks. It is, however, important to note that the drainage system currently implemented in the model uses a "simple drain" boundary condition. This boundary condition allows water to be freely removed from the modelling domain when the hydraulic head in the drain exceeds a particular prescribed threshold value. The implication of using this boundary condition is discussed later in more detail.

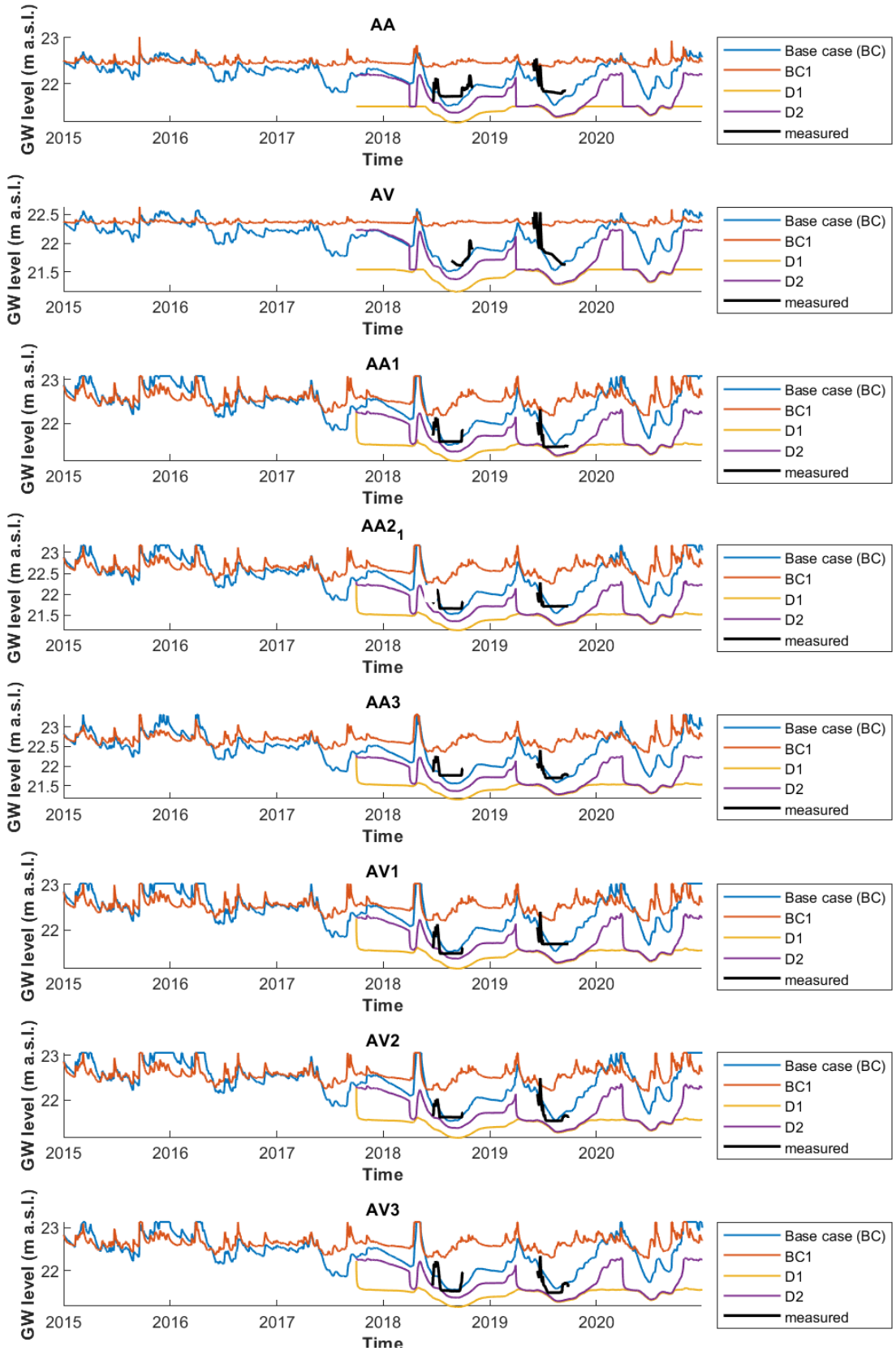

Figure 5. Times-series of measured groundwater levels and simulated scenarios at eight monitoring sites. For simplification, wells AA2_2-AA2_4 are not included in the figures.

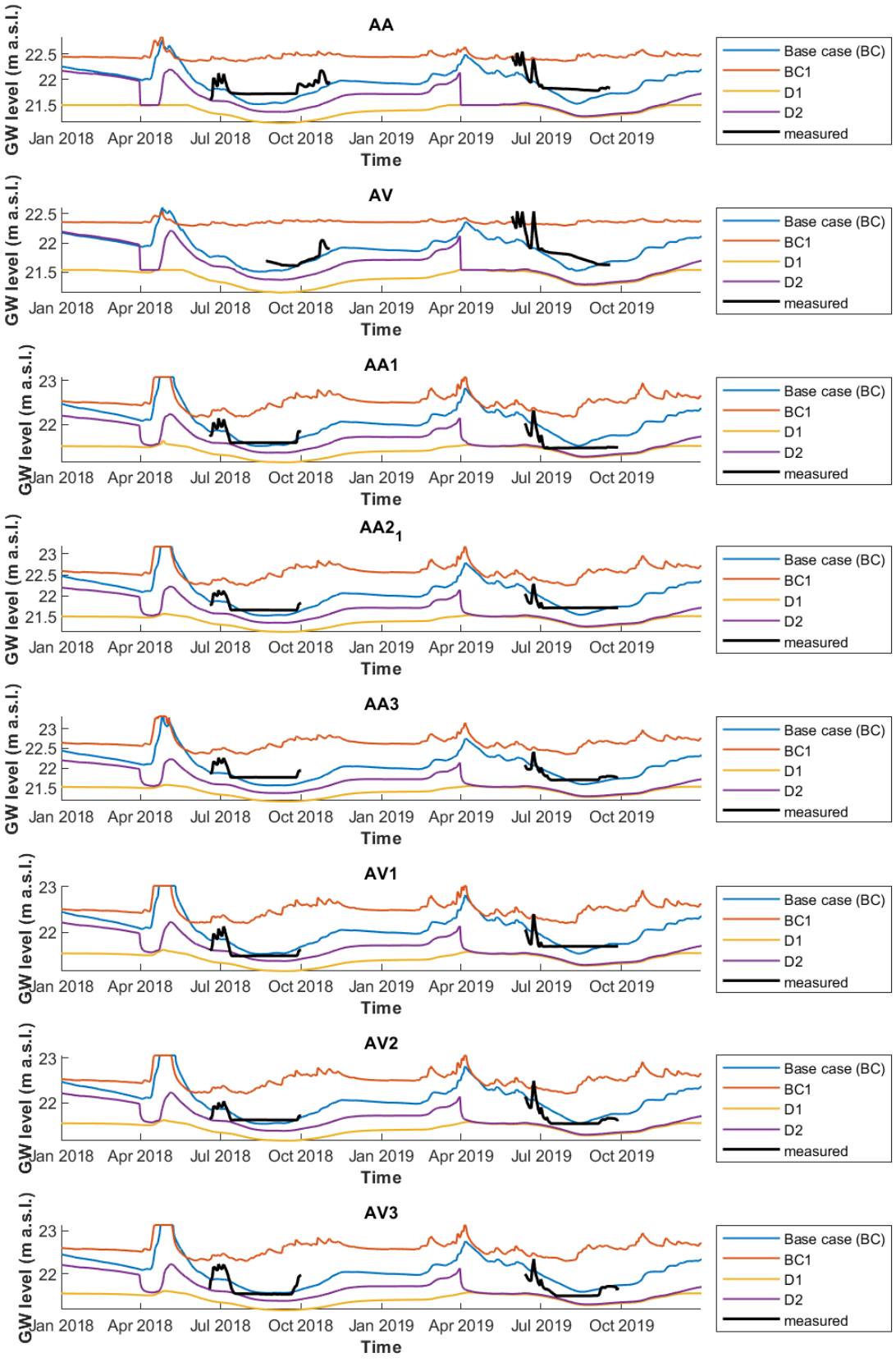

Figure 6. Times-series of measured groundwater levels and simulated scenarios at eight monitoring sites zoomed to 2018-2019 for which measurement data exists.

The impact of the control drainage system was tested by simple scheduling scheme scenario D2. The rationale for building a control drainage system is the assumption that closing the check gate allows for the rising groundwater level within the drained field. Our simulation suggests that the control drain system control over the groundwater levels depends on the environmental conditions. For instance, for dry July 2019, the closed control well system resulted in only subtly higher water table elevations with around a 3 cm difference from the traditional tile drainage system. For the year 2018 simulation, the check gate was closed earlier at the end of the snowmelt event, which resulted in the water table elevation being approximately 20 cm higher than for the case with the traditional drainage D1. These results highlight the importance of timing in the check gate closing and control well level adjustments. If the system is left to dry out during springtime, the typical summer precipitation might not be sufficient to significantly increase the groundwater table within the crop field. However, if the gate is closed when the groundwater level is sufficiently above or during the groundwater recharge event, the control tile drainage system can sustain higher groundwater levels at the field compared to what would be possible with the traditional tile drainage system.

To investigate the ability of the model to study soil moisture conditions for potato production, we plotted measured and simulated scenario D2 soil moisture in Figure 7. The HGS model output is expressed as soil saturation, defined as soil water content divided by soil porosity. In order to make variables comparable, soil water content measured with the Campbell CS616 sensor was divided by porosity values defined in the laboratory except for the data for the undersoil "jankko", which used the same porosity values subsoil because the otherwise values were over 100%. Notably, there is a relatively high spread for the sensors located at various locations for the same depth. These issues suggest variable soil properties within the field and non-compatibility of the data of this sensor type and modelling outputs in terms of absolute values. Thus, we expect some distortion but anticipate similar dynamics. The overall simulated saturations follow the same trend as the measured values, but simulated saturations are overall underestimated for the early summer and overestimated for the late summer, suggesting the evapotranspiration properties and parameterization should incorporate temporal variability. The simulated saturations also are more responsive to rainfall events seen in time series as minor spikes.

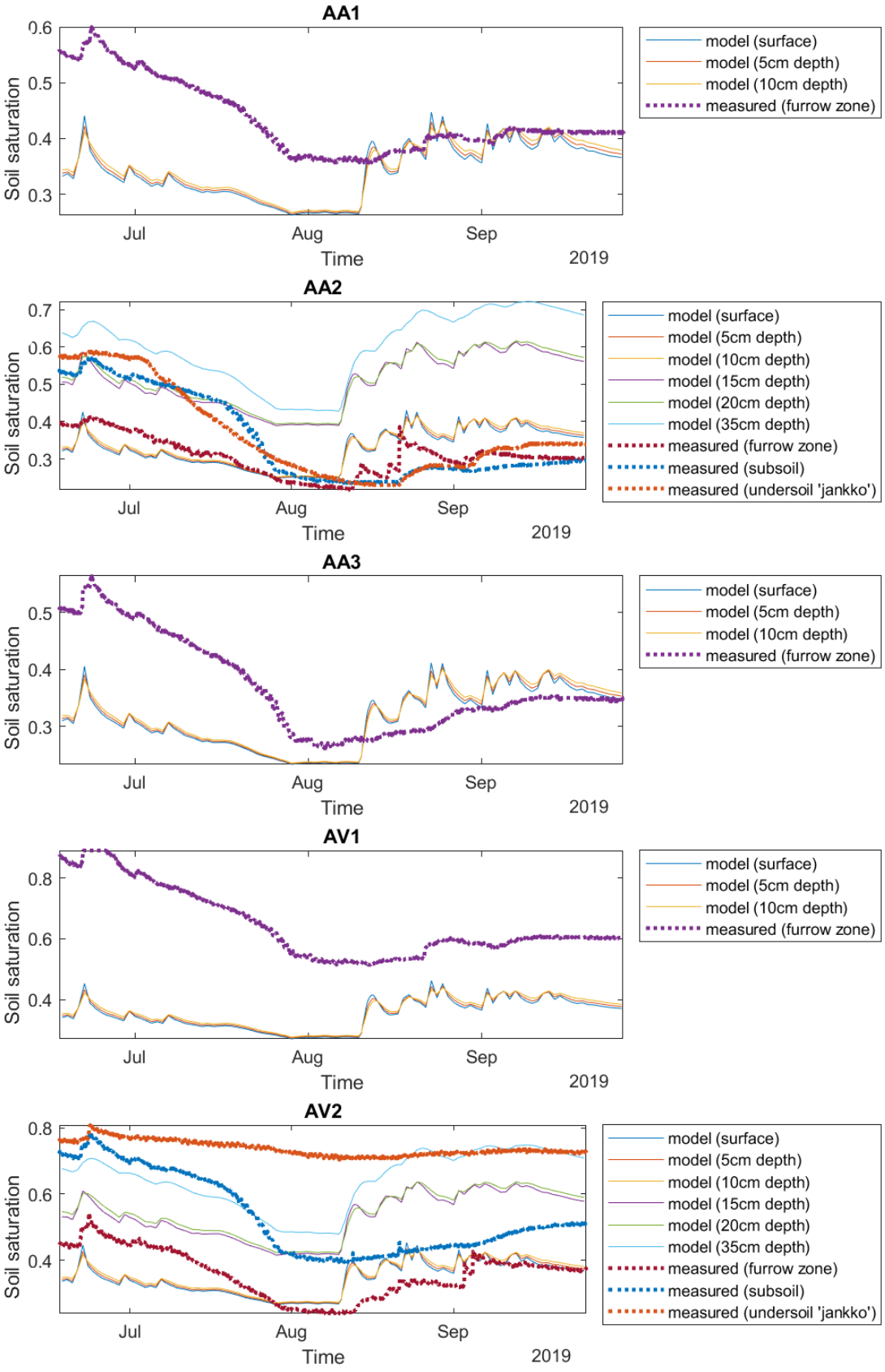

Figure 7. Measured vs. corresponding simulated soil saturations.

Scenario BC1 highlighted the sensitivity of the current model to applied boundary conditions. We further investigated the effect of various boundary conditions by three numerical tests. In Test 1, the measured hydraulic head of the control well AA for the period 21st June 2018- 11th July 2018 is applied to the tile drainage control well AA instead of 'simple drain' boundary conditions; the tile drainage at well AV discharges through 'simple drain' bound condition as in the case D2. Test 1 mimics the situation when the tile drainage system is hydraulically connected to the open ditch system. Such a situation can occur when the ditch water level exceeds the control well's outflow level. In Test 2, we applied the measured hydraulic head to the porous domain perimeter instead of no flow boundary; the tile drainage outlets discharge through 'simple drain' bound conditions as in scenario D2. This test aims to investigate the impact of regional groundwater fluctuations. In Test 3, we applied the measured hydraulic head to the overland flow domain perimeter instead of no flow boundary; the tile drainage at both wells discharges through 'simple drain' boundary conditions as in scenario D2. In Test 3, we test the impact of surface water influence in case there is no hydraulic connection between the open ditch network and the tile drainage network.

Test 1 results in Figure 8 shows that the field water table is susceptible to prescribed specified head boundary conditions; the distinct fluctuations in the water levels are reflected in all monitoring locations of the AA control drainage network and also visible as slight groundwater mounding in the AV part of tile drainage. The results of Test 2 shows that also the regional groundwater level fluctuations might affect the whole system very fast; slight fluctuations are also visible in all monitoring locations. In contrast, Test 3 indicates that in case there is no hydraulic connection, the water table elevation is little affected compared to the two previous cases. The water table rise is a few centimeters, whereas, in Tests 1 and 2, the increase is around ten times larger. These hypothetical numerical tests highlight the importance of a proper definition of boundary conditions. The influence of those on a particular field plot will depend on numerous factors, including the plot position within the catchment and site geology, but the assumption that surroundings do not influence the field plot rarely is valid.

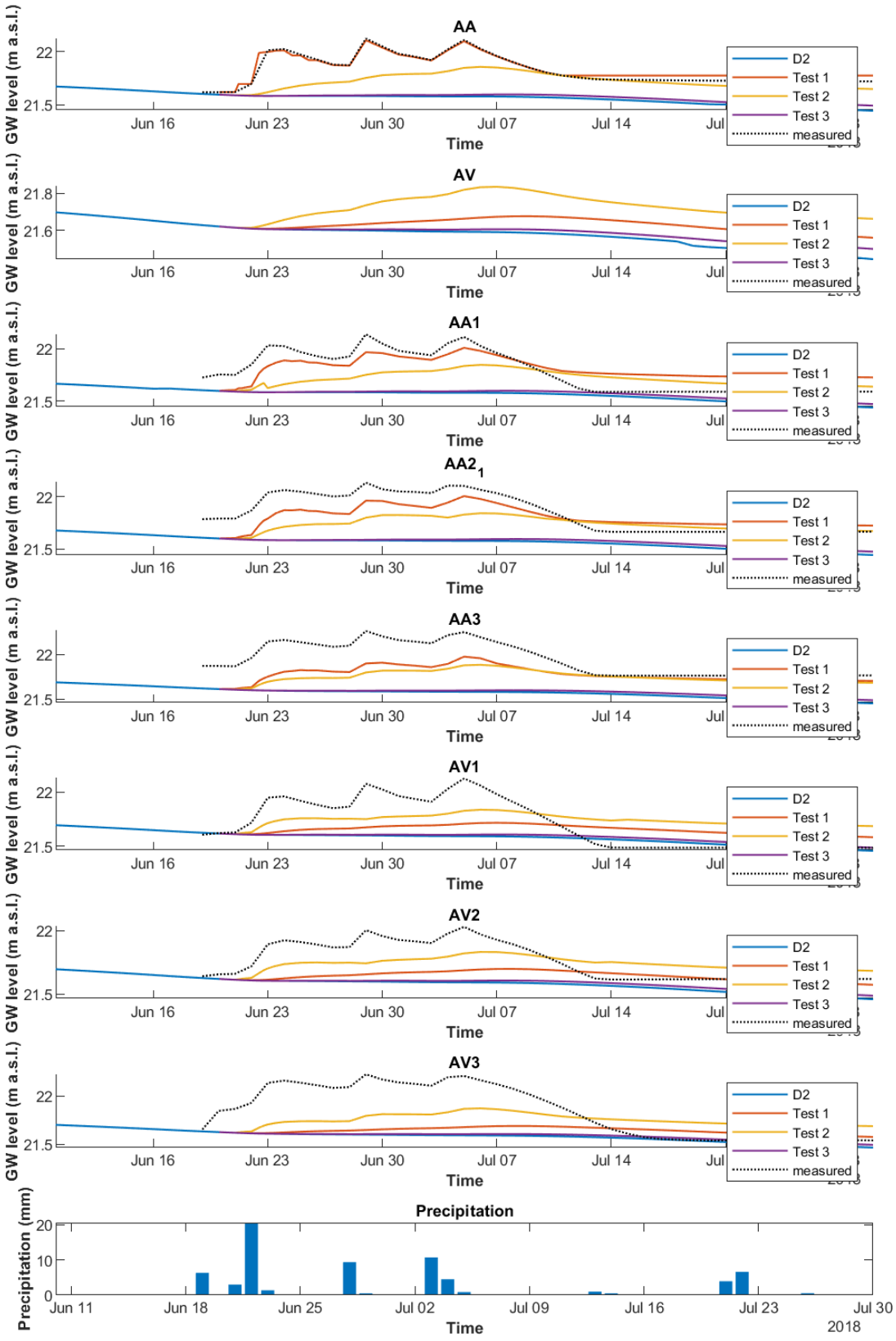

Figure 8. Specified head tests to study the impact of various boundary conditions on the tile drainage functioning in the HGS model.

Lessons learned and future model development

One should remember that the ability of the model to represent the actual system's response will depend on the quantity and quality of the data available for modelling purposes. Still, in case of limited data, physically-based numerical simulations are valuable exercises, which are the best available means to test various management practices, allow an understanding of physical processes at the site, and provide helpful insight for practices in the field conditions.

Our simulations show that the agreement between the measured and simulated base case regarding hydraulic heads is good; the general trends and magnitudes of measured groundwater levels were captured, but the dynamic and steep hydrograph rises and recession periods were missing. Still, such overall good agreement is a good proxy that model structure and chosen uncalibrated model parameters represent the system already at a satisfactory level. Thus, even this uncalibrated model version can provide valuable insights into how the system might behave under various water management scenarios. The system was responsive to the implemented traditional and controlled tile drainage systems, indicating that the HGS is a viable tool for studying the tile drainage systems' usage for optimizing soil moisture conditions.

The most important lesson we learned from the above-described modelling experiments is the importance of boundary conditions in modelling at the field scale. With no information on boundary conditions, the assumption of no flow conditions in most cases will produce inaccurate results, and the calibration will lead to over-fitting as an important hydrological driving force is missing. For this reason, meticulous attention should be put on measuring variables defining local boundary conditions in designing plot-scale field studies. It is also very important to know the control well regulation. If such data is unavailable, a model domain should be reasonably expanded outside the studied field to diminish the effect of the assigned boundary conditions. However, the application of such models is far from ideal, as the increase in the model domain size usually leads to larger system heterogeneity (more parameters) and longer model run times.

Our simulations also clearly visualized that the tile drainage system requires realistic implementation of a hydraulic connection between the open ditch system and the tile drainage outlet. Such implementation could be accomplished by switching the simple drain and specified head boundary conditions. Such an approach, however, requires an advanced technical solution similar to one required by the data assimilation procedure: The model results are evaluated after each computational timestep, and model inputs are modified accordingly, but instead of the initial conditions, the model boundary conditions are updated.

Another notable matter for consideration is DEM accuracy. Our personal experience was that available 2 m x 2 m DEM was insufficient to define the open ditch network surrounding the Tyrnävä field and resulted in undulling ups and downs and modelling convergence issues and artefacts. The tile drainage systems are usually constructed in areas in which dense open ditch network exists. Open ditch network is a relatively small-scale feature whose width is the same order of magnitude as resolution 2 m x 2 m DEM.

Finally, the field-scale model should be calibrated. Ideally, this would be done using an automatic parametrization approach, such as the model-independent parameter estimation and uncertainty analysis framework PEST (Doherty, 2010). Due to the lack of accurate information on the field scale

boundary conditions, using such a calibration procedure would be unjustified in this case and lead to the overfitting of parameters. As the main objective of this study is to define management options for the optimization of potato crop production, we propose for this study the manual calibration procedure, which would focus on capturing the main dynamics, firstly, of soil moisture and secondly, of groundwater levels and incorporating more realistic time-variable leaf area index from the satellite-derived observations.

4.2 Germany-Selhausen (T5.5): Framework for operational modelling with TSMP-PDAF and first evaluations (CLM/ParFlow)

4.2.1 Brief site description

The description for the Selhausen observatory is largely identical to the text of the official TERENO description (website) and the descriptions provided in Deliverables D7.2 and D5.2.

The German case study site Selhausen (T5.5) is part of the TERENO Rur Hydrological Observatory (Bogena et al. 2018) and represents a heterogeneous agricultural, rural area located in the lower Rhine valley (Figure 9). The mean annual temperature is 10 °C, the annual precipitation is 700 mm for the period 1961-2014, and the climate is temperate maritime. The most important crops are sugar beet, winter wheat, winter barley, maize and rapeseed. Quaternary fluvial deposits build the subsurface at the Selhausen site and are covered by loess. The major soil types are classified as luvisols and gleyed cambisols and can contain large gravel contents. The topography is flat with maximum slopes of 4° in the area of a former channel of the Rur River (local catchment).

The Selhausen site is intensively instrumented at a small scale, allowing access and use of a broad range of data for data analysis and modelling activities (Bogena et al., 2018). The Selhausen test site is equipped with an Eddy Covariance station, measuring sensible heat, latent heat and carbon fluxes and typical meteorological variables such as the three-dimensional wind component, air temperature, air humidity, net radiation (incoming and outgoing short- and long-wave radiation), photosynthetic photon flux density and precipitation (Bogena et al., 2018). An operating wireless sensor network consisting of five profiles (-0.01 m, -0.05 m, -0.1m, -0.2 m, -0.5 m and -1 m) provides measurements of soil moisture, soil temperature and soil heat flux in near-real-time (Bogena et al., 2018). The sensors host narrowband IoT modems (Wireless sensor network), allowing data transmission to a database and inclusion in a model in near real-time.

In addition, phenological developments of crops and farming activities are recorded weekly to monthly. Typical groundwater information, such as the groundwater level, groundwater electrical conductivity, and groundwater temperature, is continuously measured using a multi-parameter probe installed next to the Eddy Covariance station (Bogena et al., 2018). CO_2 emissions from the soil have been continuously measured since 2015 using four automated closed dynamic chambers (Bogena et al., 2018). Data of the described measurements are available from the TERENO Data Discovery Portal (https://ddp.tereno.net/ddp/). An overview of the location of the Rur catchment and the Selhausen site is provided in Figure 9.

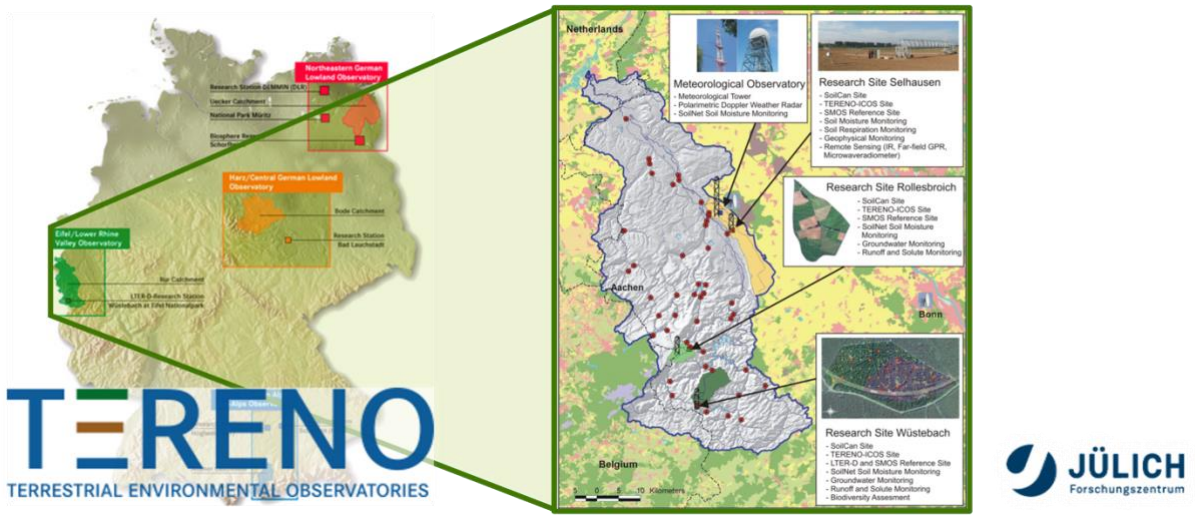

Figure 9: Overview of Terrestrial Environmental Observatories (TERENO) network in Germany (left) and close up of the Rur catchment observatories (right), of which the Selhausen case study site is a part of (image sources: TERENO & FZJ).

4.2.2 Model/Method description

In the context of D6.2, we have developed an automated pipeline for operational, site-specific soil moisture forecasting, soil temperature, crop status and other relevant variables for agricultural practice (Figure 10). For modelling at the plot scale, we use the open-source code "Community Land Model" version 5 (CLM5, Lawrence et al., 2019). We have developed a plot scale model for the Selhausen observatory that is contained in a single CLM5 grid cell (100x100x40 m) and considers 20 hydraulic active layers with vertically increasing thickness. The model is based on biophysical laws and constrained by site-specific conditions (e.g., soil texture data for different layers, land use and its change from season to season.

Vegetation states, carbon and nitrogen pools are simulated prognostically after a 1000-year model spin-up. Such a spin-up run of 1000 years takes about 6 hours on the machines of the Jülich Supercomputing Center (High-Performance Computing. The model jointly simulates water and energy transport in the unsaturated zone, crop growth and yield, snow depth and groundwater depth, and changes in carbon and nitrogen pools. We simulate past conditions using as atmospheric forcings meteorological measurements from 2011 onwards instead of atmospheric model-based data (Figure 10 c). For that, we aggregate meteorological on-site data (i.e., own measurements) mostly available at 10-minute time resolution, including precipitation, wind speed, air temperature, air pressure, relative humidity and global radiation, to 1 hour time steps to drive the model. Every calendar day, we simulate future conditions, e.g., site-specific soil moisture information, for the next 10 days, using as atmospheric forcings weather forecasts from the German weather service. Simulations for the past and the future can be performed relatively quickly, and results can be provided in less than an hour.

Currently, forecasts start only from initial conditions obtained from forward simulations, i.e., states generated from simulations without a data assimilation step (Open Loop). However, the assimilation of site-specific soil moisture data step in near-real time is being developed at the time of this report. This will allow for uncertainty quantification and allow the use of a less uncertain initial condition for site-specific operational soil moisture forecasting. In addition, we will conduct predictions using

climatological mean time series and available climate scenarios as atmospheric forcing. Available land use scenarios could also be considered.

Ideally, model-generated information could be used by farmers to plan irrigation and drainage and estimate trends in crop development and yield. For D6.2, we mimic the operational near-real-time modelling based on sensor information and weather forecasts at Selhausen for January 2022. Simulations based on data assimilation will be presented separately in D7.5. We are releasing the generic scripts that will allow site-specific models to go live with and without data assimilation for other sites in about a day.

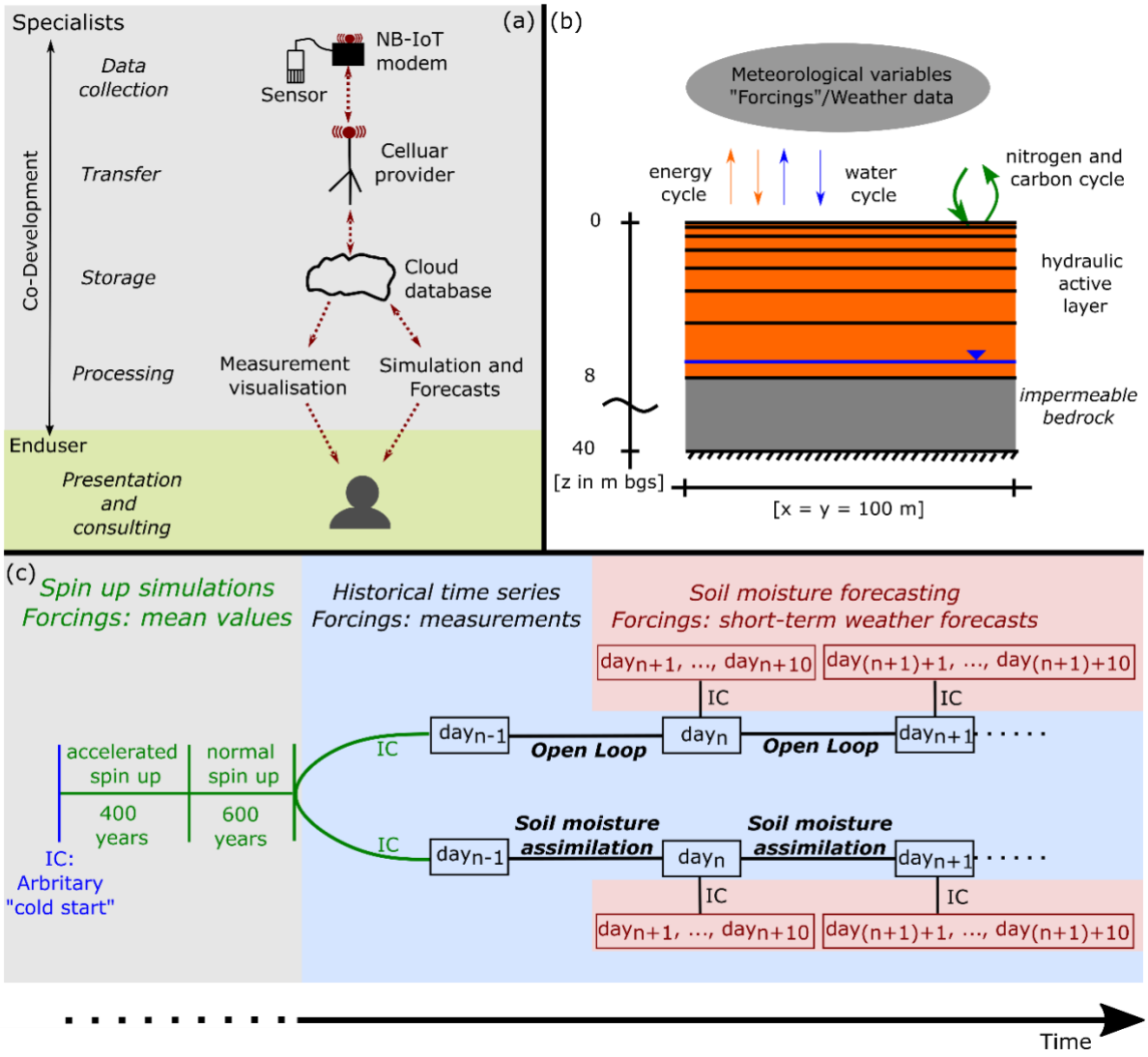

Figure 10: Automated data pipeline for operational site-specific soil moisture ensemble forecasts (Hoffmann et al., in prep. for GMD). (a) Scheme for data transmission from sensors to the end user; (b) Conceptual model for a plot-scale model of Selhausen; (c) Simulation routine for daily forecasts of the hydrologic, crop, carbon, and nitrogen conditions and fluxes for the next 10 days.

4.2.3 First results

Exemplary, we show soil moisture forecasts for the next days starting on January 1, 2022, using as atmospheric forcings weather forecasts from the German Weather Service (Figures 11 and 12). The

simulation of soil moisture dynamics at the plot scale can be improved when weather forecast uncertainties are considered, adding to precision irrigation and optimizing irrigation schedules while keeping crop productivity stable.

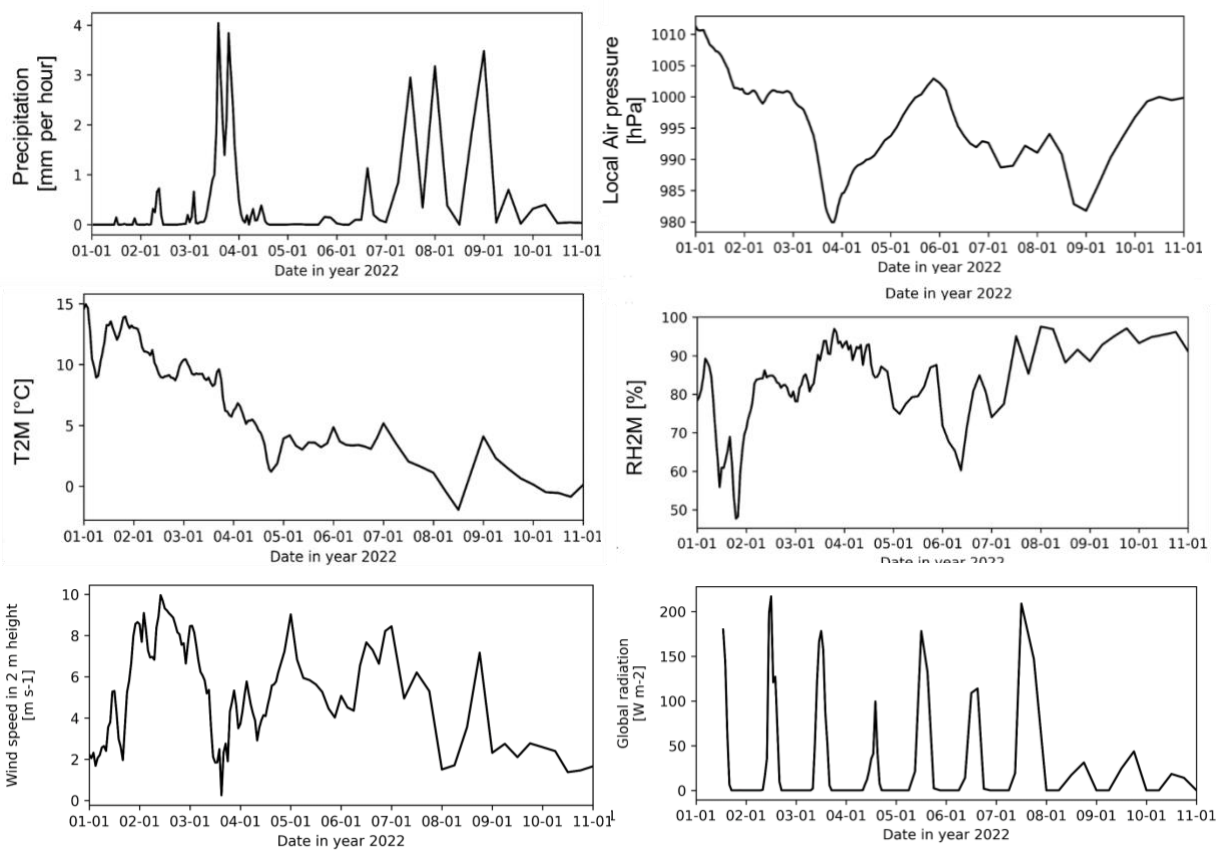

Figure 11: Weather forecast from the German Weather Service aggregated to the model time step and grid cell size.

Until now, the initial condition of the forward model is only based on forward simulations. However, we are performing simulation experiments with and without data assimilation and with and without parameter estimation. For that, the Parallel Data Assimilation Framework (PDAF) has been coupled to CLM5 (Strebel et al., 2022), and CLM5-PDAF is being applied to the Selhausen site. In a data assimilation approach, an ensemble of model runs is performed, which captures the model uncertainty and provides an initial condition for our forecast model with reduced uncertainty. We will assimilate measurement data from in-situ and remote (satellite) sensors (e.g., soil moisture, leaf area index) that will be used to correct the simulated model states in near real-time so that these are closer to the measured values, also taking measurement uncertainty into account. The data assimilation step allows uncertainty quantification and reduces typically prediction uncertainty. An ensemble of 50 medium-range weather forecasts from the German Weather Service drives CLM5-PDAF in forecast mode. This produces predictions of hydrological conditions (e.g., soil moisture contents), crop conditions (e.g., biomass, plant drought stress), energy cycles (e.g., soil temperature) and carbon and nitrogen pools and fluxes for the next two weeks with reduced uncertainty. Forecasts starting from initial conditions based on soil moisture assimilation will be more reliable for stakeholders as model bias is reduced.

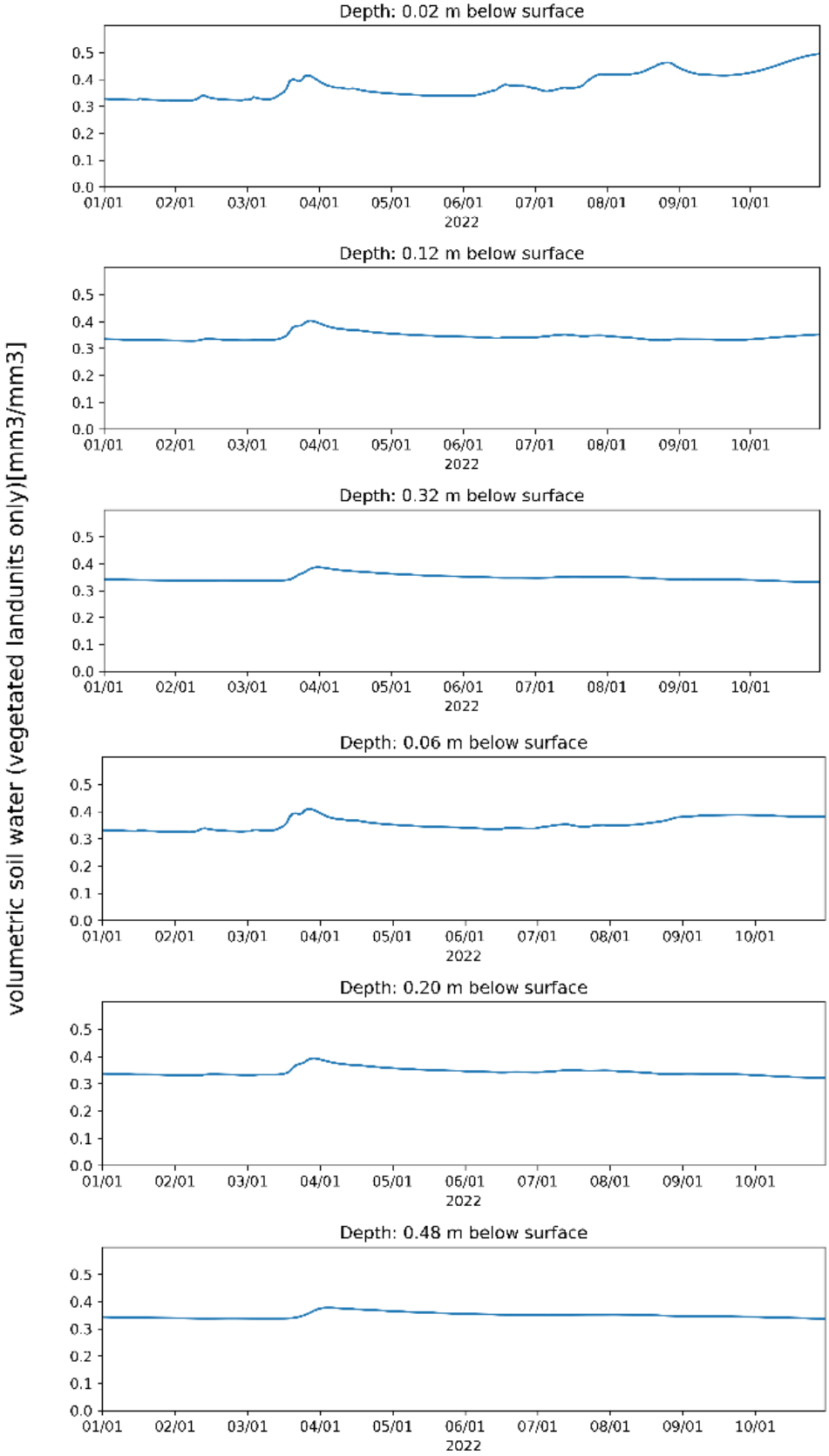

Figure 12: Site-specific 10-day soil moisture forecasts for different soil depths using weather forecasts from the German Weather Service (Figure 11) as atmospheric forcings in CLMv5 (single grid cell model).

4.3 Poland-Lower Silesia (T5.6): Model-based evaluation of water retainer (HGS) (UPWR/UNINE)

4.3.1 Brief site description

The Lower Silesia agricultural case study site is located in South-West Poland around Lubnów village, which is approximately 20 km North of Wrocław. In hydrological terms, the studied farm is located on the border of two different hydrological catchments. However, as 90 % of the area of the farm is located in the Ślęganina river catchment, only the Ślęganina river catchment was considered for the fully coupled and physically based modelling experiments. The Ślęganina river is a tributary to the Odra River, which is Poland's second-largest river. The entire surface area of the catchment is 17.4 km^{2,} but for modelling purposes, the catchment was limited to the 14.6 km^2 to model the catchment outlet around the location of the installed limnimeter (roughly 500 m upstream from the joint of Ślęganina and the Odra rivers). According to the climate classification by Okołowicz (1977), the climate of the catchment is temperate warm transitional. The modelled Ślęganina river catchment and the currently implemented numerical grid are illustrated in Figure 13.

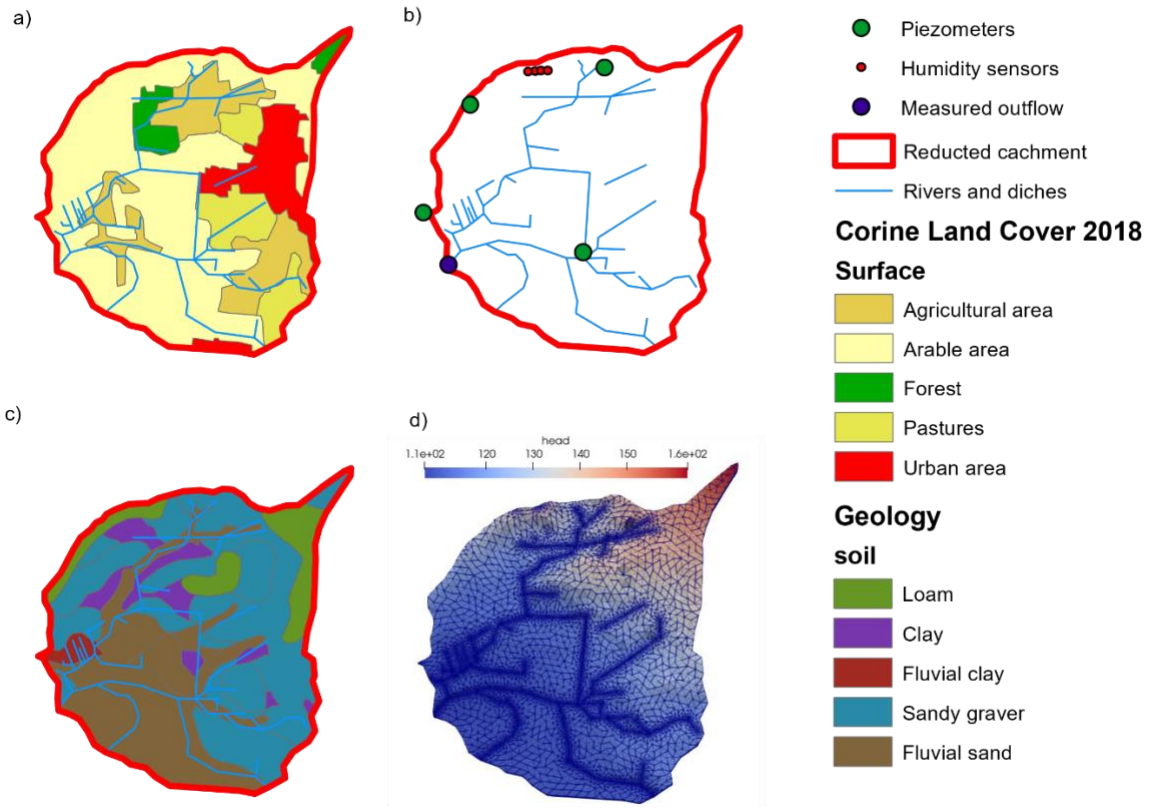

Figure 13: Maps of land cover (a), measurement network (b), soil types (c) and conceptual 3-D model of the catchment generated with HGS (d).

The mean annual precipitation at the study site, measured over 1991-2020, was 541 ± 95 mm. The mean air temperature over the same period was 9.7 ± 1 °C. With an average depth to groundwater,

table of 1-2 m, a significant amount of groundwater resides in the shallow aquifer of the study site. According to the information obtained from 20 boreholes, the shallow aquifer is limited underneath by impermeable bedrock sitting at a depth of 2-5 m, depending on the location within the catchment. The catchment area is covered with topsoil consisting of loamy sand (about 80 % of the area), clay (15 %) and silt (5 %). Below the depth of 3-3.5 m, the soil is mainly composed of clay.

4.3.2 Model description

Two models are developed with HGS:

1. *1D model* for rapid Water Retainer assessment.
2. *3D catchment model* (Figure 13) for assessing irrigation water demand under different climatic and agricultural land use scenarios.

Both models run as physically based and fully distributed integrated surface-subsurface hydrological models (ISSHM).

Description of 3D catchment model:

The currently implemented numerical model grid consists of an approximately equilateral triangular mesh with 18 608 nodes and 36 948 elements of variable size with higher resolution along agricultural drains and ditches and lower resolution on agricultural fields (Figure 13d). Vertically, the model was discretized into 16 layers employing proportional sub-layering, whereby each of the top 10 layers was set to cover 2.5 % of the total vertical extent of the model at any location, and the bottom 6 layers to cover 12.5 % each. This fine vertical discretization in the top 25 % of the model guarantees a numerically accurate simulation of variably saturated flow processes as required by Richards' equation (Downer and Ogden, 2004).

4.3.3 First results

Monitoring data [preliminary]

In November 2020, 4 piezometers and 4 soil moisture measurement stations were installed in the studied catchment. The soil moisture stations measure the soil moisture within the top 80 cm of the soil at 10 cm intervals. As mentioned above, the limnimeter is located at the outlet of the catchment, while the meteorological station is situated in the upper part of the catchment. The measurements will be continued till the end of the project to enable the full assimilation of data with the 3D model, which is under development.

1-d model for Water retainer assessment [preliminary]

The Water Retainer (WR) product was applied on 1 ha plots with oats (2021 vegetation period, sandy soil), wheat and barley (2022 vegetation period, loamy sand). It resulted in 7 %, 11 % and 33 % increase in yield compared to untreated plots, respectively.

Simple 1-D models were made for all scenarios with and without WR application (4 with oats, 2 with wheat and 2 with barley). It was observed that WR affects soil properties during the first 3 months after application (Figure 14).

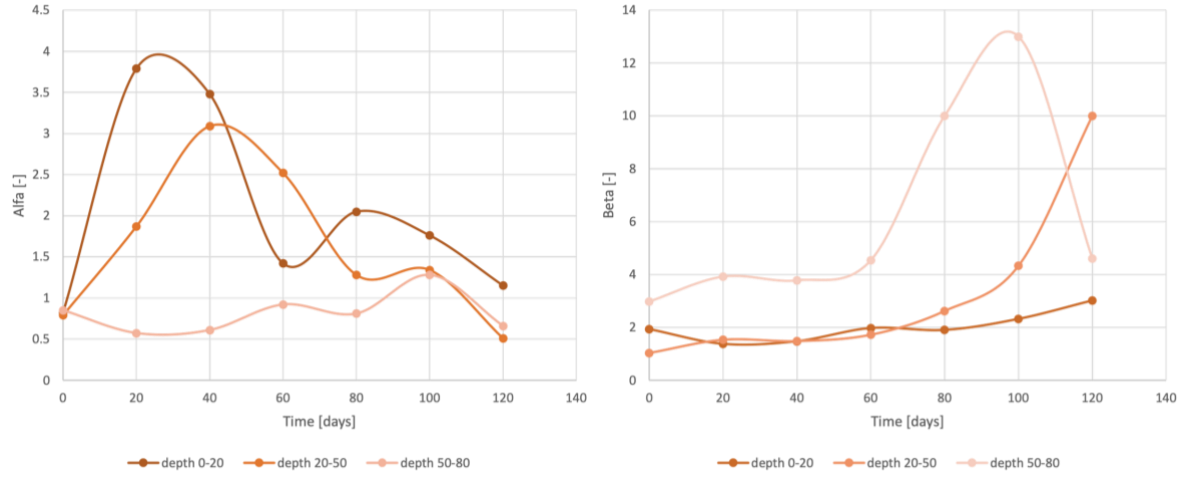

Figure 14: The influence of WR on variability of Van Genuchten parameters alfa and beta obtained from 1-D models in HGS.

Soil moisture content was continuously measured at different depths for each variant of WR application and outside the area sprayed with WR. The field water consumption method was used to assess the effectiveness of the WR. Detailed results are presented in Deliverable D3.2: Assessment of Water Retention Methods.

It is planned to test at least 3 other 1D columns located in different fields to create a pedotransfer function that describes the change of soil properties over time under the effect of WR.

Catchment model [preliminary]

To illustrate the current state of the physically-based modelling at the Lower Silesia case study site, the existing model was used to simulate 3 key meteorological scenarios: the year which most closely reflects the annual average precipitation as measured between 1991 and 2020 (2005; 544.5 mm of precipitation), as well as the driest (2015; 388.2 mm of precipitation) and the wettest (2020; 736.5 mm of precipitation) years during the same reference period.

Simulations were run for a full 365-day period, driven by daily precipitation sums as measured during the respective years. As remote sensing-based high-resolution maps of vegetation covering will only become available for the Lower Silesia case study site later during WP3/the WATERAGRI project, evapotranspiration was not explicitly simulated, and instead the actual measured daily evapotranspiration was subtracted from the actual measured daily precipitation prior to force the model. Winter hydrological processes, such as snowfall and snowmelt, were not explicitly considered, and all precipitation was simulated as rain. Illustrations of the subsurface saturation of the physically-based model under the three scenarios are presented in Figure 15.

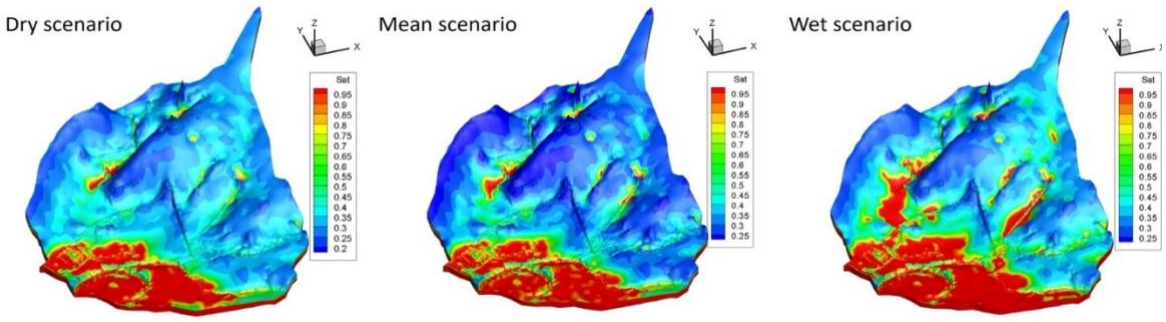

Figure 15. Comparison of subsurface saturation in the catchment on an arbitrarily chosen day (day 200 = 18 July)

It is planned to use a novel pilot point method for catchment calibration where soil conductivity will be calibrated according to water level measurements in piezometers, the soil moisture content in the top soil and water stages registered by the limnigraph.

4.4 Switzerland-Seeland (T5.7): Drainage control based on HGS-PDAF (HGS) (UNINE)

4.4.1 Brief site description

(The text below is largely identical to the text of the Seeland site description in Deliverable D5.1)

The Seeland (Figure 16) site is Switzerland's largest vegetable farming area. It is characterized by very fertile peat soils, which are extensively used for farming. The Seeland has historically been subject to major floods. Three major, regional scale water correction projects carried out in the last 150 years reduced the flood risk and made the region arable. The corrections included the construction of several canals, an extensive drainage channel network to lower the groundwater table and the redirection of major waterways away from the heart of the Seeland, resulting in a much more predictable and manageable agricultural landscape ideal for vegetable farming. However, the lower water tables in the peat-soils greatly increased the decomposition of organic matter, resulting in a loss of up to 1.6 meters of soil. The remaining fertile peat soils now represent a scarce resource in urgent need of protection. If current agricultural practices are continued, soil resources will be depleted in the next 10-15 years.

Figure 16: Location of the agricultural area 'Seeland - Grosses Moos' within Switzerland, outlined in orange (left), and view of the study field (right, outlined in red).. Image source: Google earth.

4.4.2 Model/Method description

A surface-subsurface model is being developed by HGS for the Seeland test site. The goal of the model is twofold: We use it as a test site to explore to what extent water management can be improved under consideration of agricultural efficiency and conservation of soil. Specifically, we can test to what extent the joint management of the operation of the drains and the regulation of the water level in the surrounding channels can be used to maximize efficiency. In addition, a parallel, ensemble-based data assimilation system, HGS-PDAF, is being developed to facilitate real-time operational simulations of water quantity and quality.

Figure 17 shows the overview of the domain size and the topography of the model of the Seeland site. The model is discretized in the horizontal direction by triangles composed of nodes with inter-nodal spacing ranging from 5 to 15 m, resulting in 21 903 elements and 11 219 nodes per layer. In the vertical direction, the model is divided into 19 layers at depths of 0.15, 0.30, 0.45, 0.60, 0.75, 0.90, 1.05, 1.20, 1.50, 2.0, 3.0, 4.0, 5.0, 6.0, 7.0, 8.0, 9.0 and 10.0 meters. The depth for the bottom layer is at 15 meters. The model is constrained by three open channels simulated as head-dependent boundary conditions. Recently created 3-D subsurface maps of soil hydraulic properties are implemented in the model to significantly improve the representation of heterogeneity in the vadose zone.

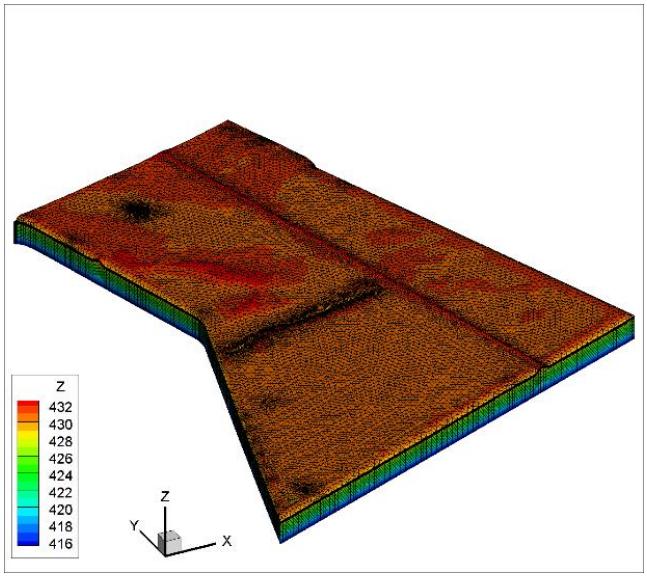

Figure 17: Numerical grid with high-resolution topography shading of the physically-based model of the Seeland case study site

The available drainage network is located in the top 1-2 meters of soil. Drains are dewatered via water level management in the surrounding channel network. These drains help maintain soil stability by removing excess water from the soil and maintaining the proper water levels in the soil for optimal plant growth. However, the soil water content is often too high in the region's centre (see Figure 19, left). To prevent waterlogged conditions, new drains are developed and included in the existing drainage system in the model and the test site (see Figure 18). These newly added drains in the field can be switched on/off depending on the requirement of the farmers.

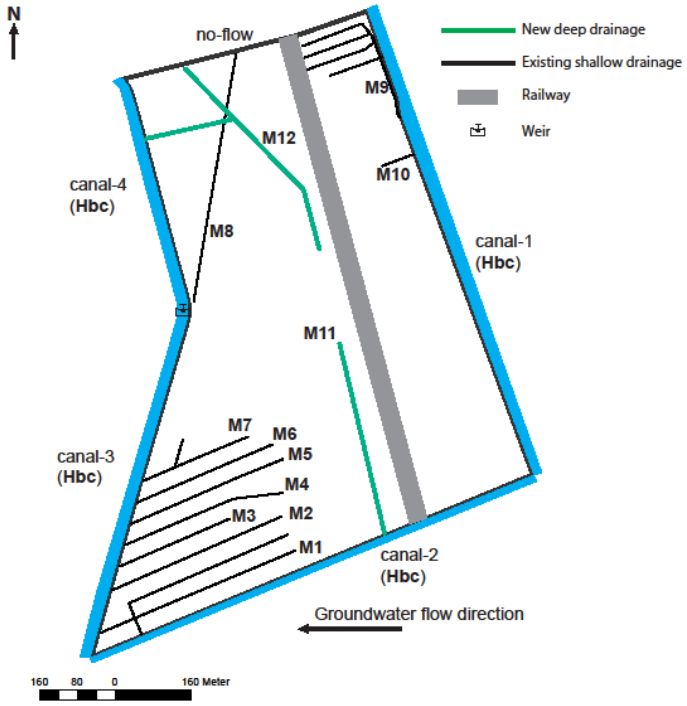

Figure 18: Drainage system in the Seeland site

DA Framework: HGS-PDAF

Parallel to developing the HGS model, a new data assimilation framework is being developed for HGS. The data assimilation module is based on PDAF, which allows state-of-the-art data assimilation algorithms. The newly developed HGS-PDAF system consists of four modules: the HGS executables, the PDAF source code, the model bindings, which are a set of user-specified subroutines that act as an interface to the PDAF source code, and the 'driver' to manage the data assimilation simulation runs. The driver can be written as bash or python scripts. PDAF allows the application of several types of observations that can be assimilated together or separately. This is achieved by implementing the observation modules for each observation type separately.

Similarly, the combination of variables in the state vector can be flexible. So far, the joint assimilation of several types of observations, such as piezometric head and soil moisture, is possible with the current version of the developed DA system. The state vector can include the model simulated states (e.g. hydraulic heads and water saturation) and the model parameters (e.g. hydraulic conductivity).

4.4.3 First results

The numerical model was run with a constant forcing to qualitatively evaluate the effects of the new deep drainage system on the soil water saturation (see Figure 19) and the influence of managing the water tables in the channels. Overall, it is possible to see the beneficial influence of the deep drainage system on the water saturation in the field, as the presence of the deep drainage significantly reduces the soil water saturation in the vicinity of the drainage location. These preliminary results illustrate that the proposed active drainage control efficiently the soil water saturation.

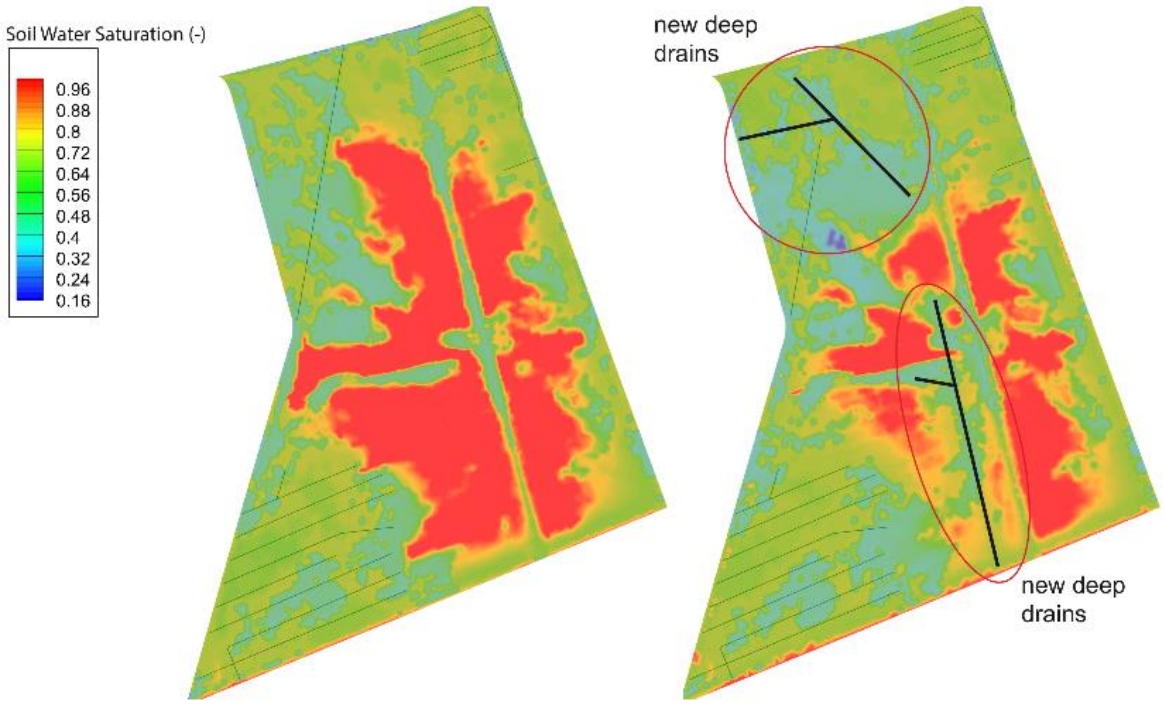

Figure 19: Model outputs (water saturation) without drains and with the new deep drainage. Warmer colours indicate soils with high saturation and colder colours indicate soils with low saturation.

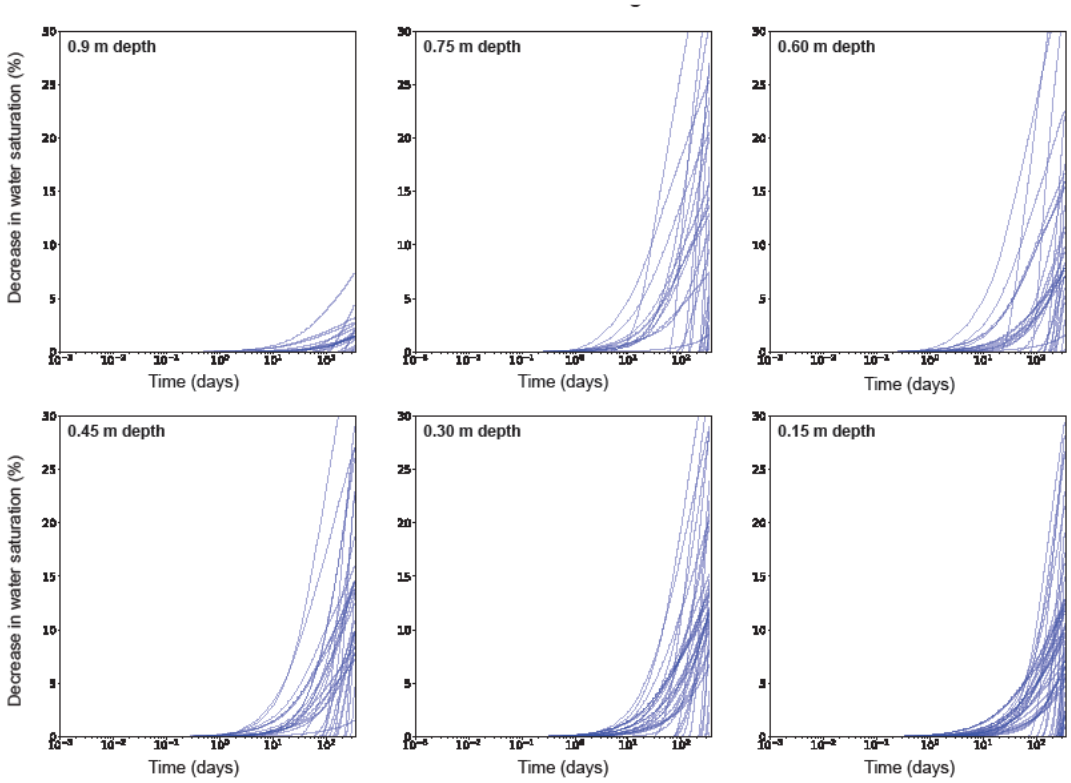

Figure 20: Cumulative decrease in water saturation at different depths in time.

With this new drainage system, we further monitor the saturation variation of the test site when the water levels in the boundary canals are decreased by one meter. Figure 20 shows the decrease of water saturation in the subsurface down to 0.9 meters in blue lines. These different lines represent different model nodes along the middle of the region. The saturation decreases more and faster in the layer close to the surface than in the deeper layer. Below 0.9 meters is a fully saturated zone where no saturation variation is observed.

The simulations clearly show that the soil-aquifer system is sufficiently reactive to substantially influence the soil water conditions through targeted drain and channel management. This is the precondition for the real-time simulation, which is currently being developed.

4.5 Hungary-Nyírbátor (T5.10): Irrigation scheduling (CLM5) (UNIDEB/FZJ)

4.5.1 Brief site description

The study area is situated in the Pannonian region with a continental climate, at the Northern Great Plain region in Szabolcs-Szatmár-Bereg county, next to Nyírbátor city (47°48'18.60"N, 22° 9'43.89"E) (Figure 21), which has a moderately cool and dry climate in Hungary. (Figure 21). The case study site is in a nitrate-sensitive area (based on European guidelines) and owned by a private company: Bátortrade Ltd. The case study site comprises 16 ha of pasture with sprinkler irrigation (on fixed hydrants) for cattle grazing and 50 ha of irrigated arable land with a lateral moving irrigation system for feedstocks. The case study site is situated at an alluvial cone plain covered mainly with sand. The

area's current rivers and partially deflated wetlands are indications of the region's historically rich water network, but its active water network is limited, so its horizontal fragmentation is modest. The micro-region is characterized by parabolic sand dunes and closed depressions, which are also found at the case study site. The altitude of the pasture site is between 151 and 156 m; for the site with the lateral moving sprinkler irrigation system, it is between 146 and 150m. The average annual amount of sunshine hours is around 1875, with approximately 750-780 hours in the summer (June- August) and 165-170 hours in the winter (December-February). The area's wind averages 2.5 m/s, and predominant wind directions are north and southeast. In summary, the case study site with no irrigation is suitable for drought-tolerant species and varieties with lower water demand.

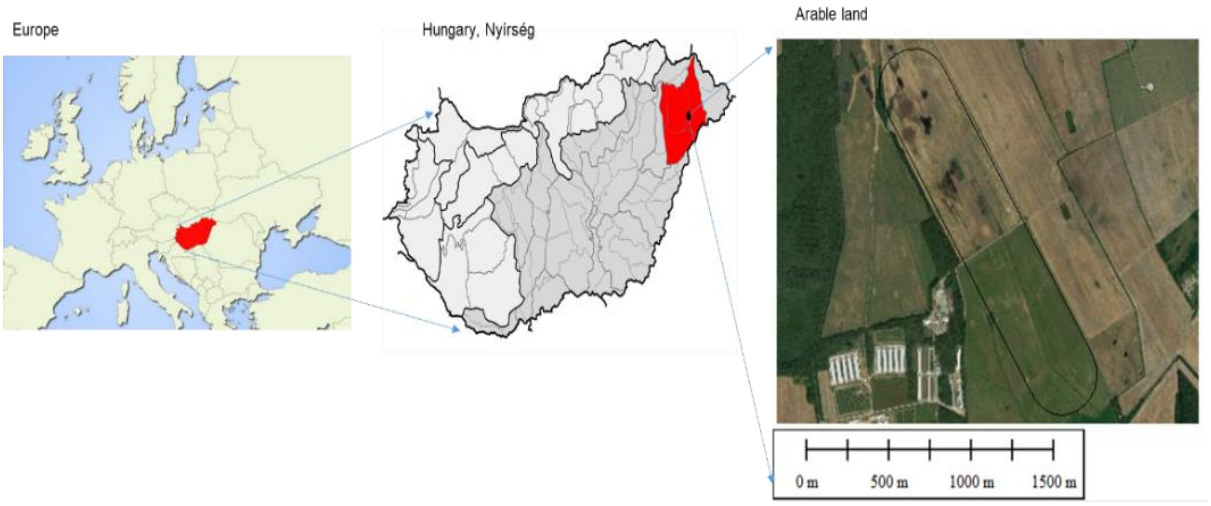

Figure 21: Location of the meteorological research station Nyírbátor in eastern Hungary.

4.5.2 Model/Method description

For the Nyírbator site, a one-grid cell model for optimizing irrigation scheduling is being developed using the Community Land Model version 5 (CLM5). CLM5 is a land surface model, and its main features were described earlier in this deliverable.

Here a physically based CLM5 model for the Nyírbátor site was set up, simulating hydraulic and plant conditions for 2020 and 2021. The model mesh consists of a single grid cell with a size of 100x100x40 m and considers 20 hydraulically active layers with increasing thicknesses. The coordinates of the Nyírbátor weather station form the grid cell centre. The grid cell is bare soil during winter and rain-fed corn in summer. Later simulations with irrigated-fed corn are planned. The observation period is simulated starting from the 1000 year spun-up states. The spin-up run initialises vegetation, carbon, and nitrogen pools. On-site instrumentation provides measurements of precipitation, wind speed, air pressure, air temperature and relative humidity with a time step of 1 hour, and global radiation as a daily average (Figures 22 and 23). All meteorological observations were aggregated in daily time steps to match the temporal resolution of global radiation. We used these observed meteorological conditions as atmospheric forcings and used them to simulate the years 2020 and 2021, starting from the conditions at the end of the spin-up phase. The calculation time step was 1 day, like the temporal resolution of global radiation. Other input parameters are aggregated from high-resolution input data sets to the model grid cell and time step, as typically performed by CLMv5 users.

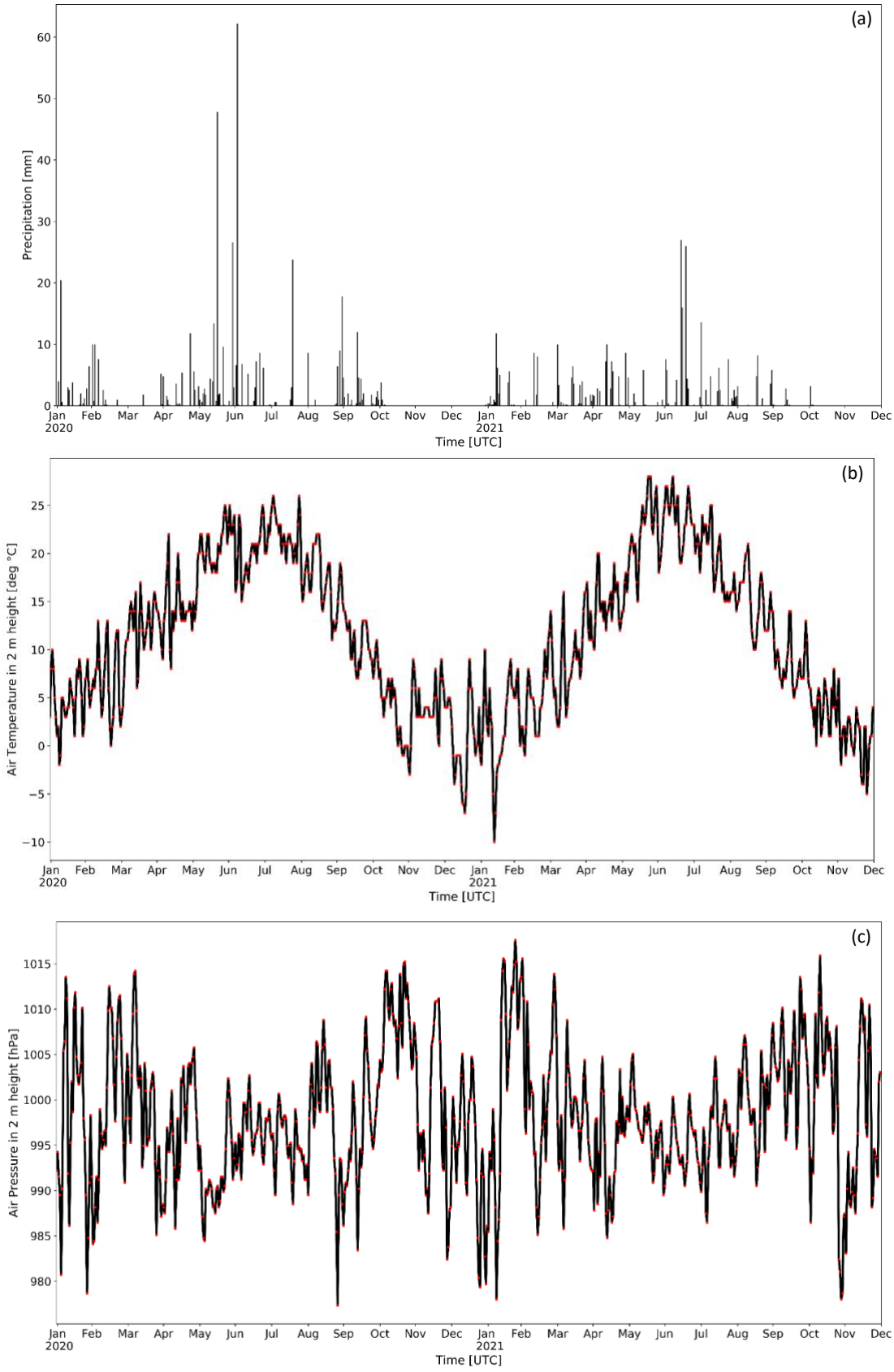

Figure 22: Input atmospheric forcings for the CLM5 model of the Nyirbator site: (a) Daily precipitation; (b) Daily average air temperature (c) Daily average air pressure.

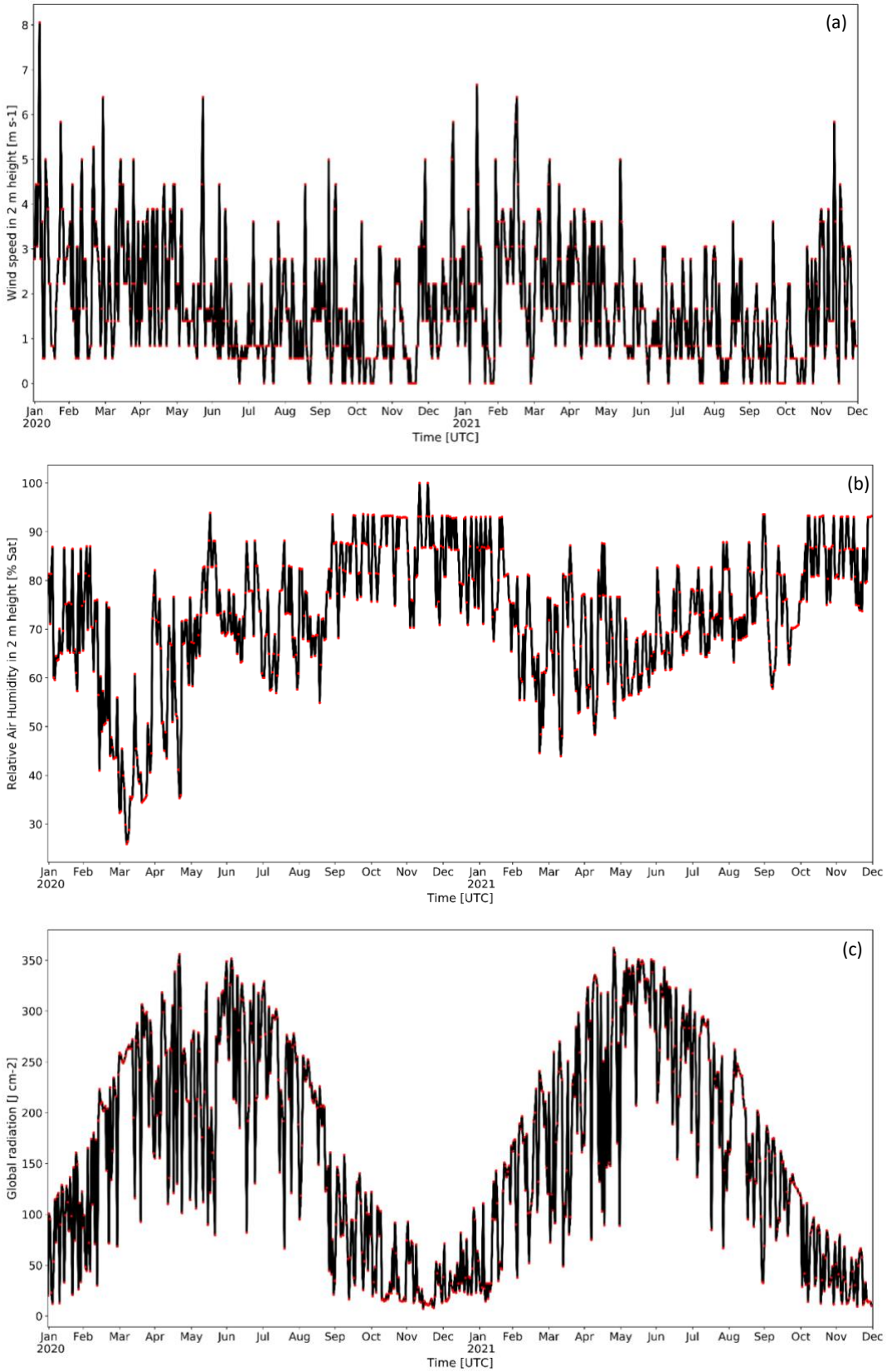

Figure 23: Input atmospheric forcings for the CLM5 model of the Nyirbator site: (a) Daily average wind speed; (b) daily average relative humidity; (c) daily global radiation.

4.5.3 First results

Figure 24 shows an example of the simulated soil moisture and soil temperature as a function of time for a depth of 10 cm. Soil moisture at 10 cm depth ranges from 6 to 30 %, which is typical for the region. Precipitation in July 2021 was anomalously low, and 2021 was an anomalously dry year. Consequently, simulated soil moisture values are lower in 2021 than in 2020. The soil temperature at a depth of 10 cm was around 260-300 Kelvin. The soil temperature in the area was high in summer, related to high air temperature and low soil moisture contents.

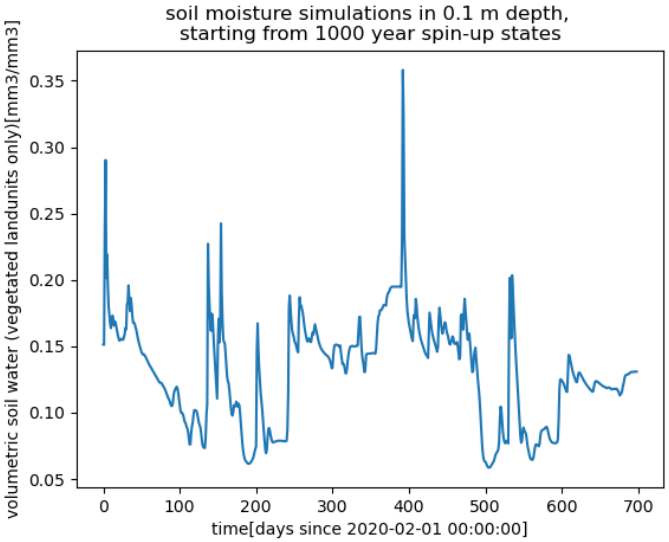

Figure 24: Simulation of soil moisture at 10 cm depth

The model is designed to optimize irrigation scheduling and support agriculture decision-making. Therefore, we plan simulations with irrigation-fed corn and estimate irrigation needs with our CLM5 model. Models estimated for irrigation needs in 2020 and 2021 will be compared with records of irrigation rates provided by local farmers. In the next step, the model will be extended to also allow forecasts.

4.6 Method to derive soil hydraulic properties (USAL)

4.6.1 Method description

I. Experiments

Two experimental tests assessed the water retainer effects on the soil water retention curve and soil water diffusivity. The water retention curve test was conducted using an environmental chamber to control the relative humidity to which the soil samples were exposed until reaching equilibrium states when no sample weight change was observed on the scale of accuracy 0.02g, as shown in Figure 25(a). The controlled relative humidity exerts a certain suction on the pore water in the soil samples, which is evaluated in terms of the Kelvin equation (Fredlund, 1989):

(a) (b)

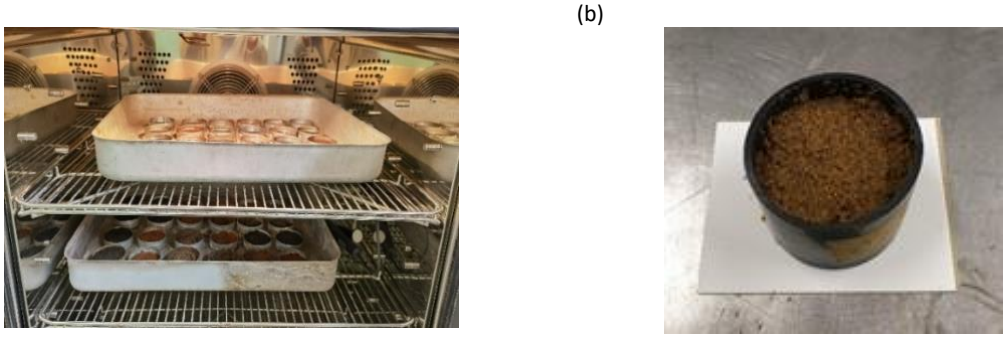

Figure 25: Experiments to determine soil hydraulic properties, (a) water retention test, (b) water diffusion test.

$$\psi_m = -RTln(RH)/V_w$$

where ψ_m is the soil matric suction (Pa), R is gas constant (8.314 Joule/K/mol), T is the temperature (K) (set as room temperature 293°K), RH is relative humidity, V_w is the water molar volume, which is about 18.03×10^{-6} (m^3/mol) at room temperature. Figure 26 gives out the suction values using the relative control approach.

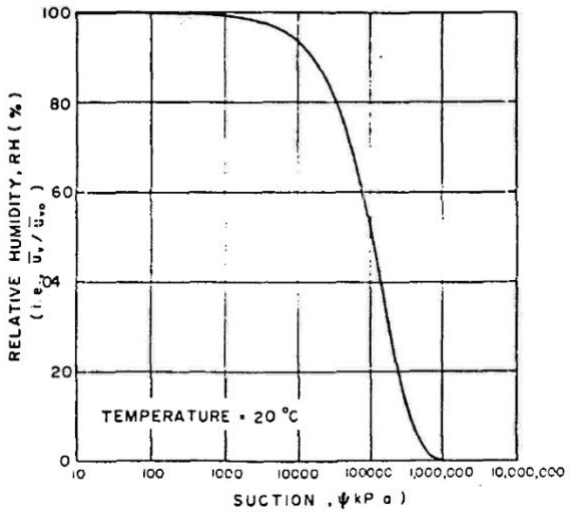

Figure 26: Relationship Between Relative Humidity and Soil Suction

(Delwyn D. Fredlund, 1989, Soil Suction Monitoring For Roads And Airfields, SYMPOSIUM State-of-the-Art of Pavement Response Monitoring Systems for Roads and AirfieldsAt: West Lebanon New Hampshire USA)

The water content at the equilibrium states was measured by weighting. The water retention curve was measured by a drying process starting from fully saturated. The pore water of each soil sample has a certain water retainer concentration, which was 0%, 1%, 2%, 3% and 5%, respectively, by the pore water volume at a fully saturated state. Three types of soil were tested, they were: 1) sand, 2) clayed sand A (70% sand & 30% clay) and 3) clayed sand A (50% sand & 50% clay). They had an estimated porosity of 0.26, 0.28 and 0.35, respectively. Figure 27 compares the initial measured water to dry soil weight ratio (w/s) at the start fully saturated state of the three soils. A fully saturated state is set at the point where there is no draining free water (using paper towel to dry the top surface of the samples filled in cylindric containers). The results show that for each of the soils the measured fully saturated water content increases with the increased use of water retainer. The results can be interpreted as that if we set the saturated state of the soil samples, which has no use of the water retainer (0% WR), as the benchmark for the just saturated state of soils, the use of the water retainer will keep the soils over saturated under same environmental exposure. This gives the 1st evidence for the effect of the water retainer.

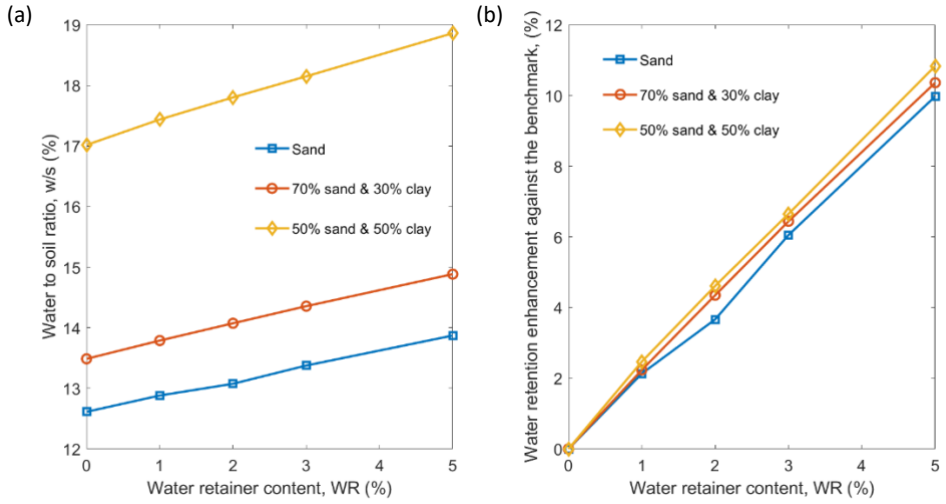

Figure 27: (a) the water to dry soil ratio at the start saturated states, (b) the water content increasement against the benchmark (WR = 0%).

All following measurements under relative humidity control were taken at equilibrium states. An equilibrium was assumed when the weight of the samples had no change (or precisely change is less than 0.02g) for at least one week when exposed to certain relative humidity values inside the environmental chamber. Figure 28 shows the measured equilibrium water content (water to dry soil ratio) at 7 controlled RH magnitudes; they are 90%, 75%, 60%, 45%, 30%, 20%, 10% and oven dried (set as 0.001%). The results demonstrate the water retainer (WR) effect on soil water retention enhancement, i.e., the higher the WR concentration, the higher the soil water content at the same suction value.

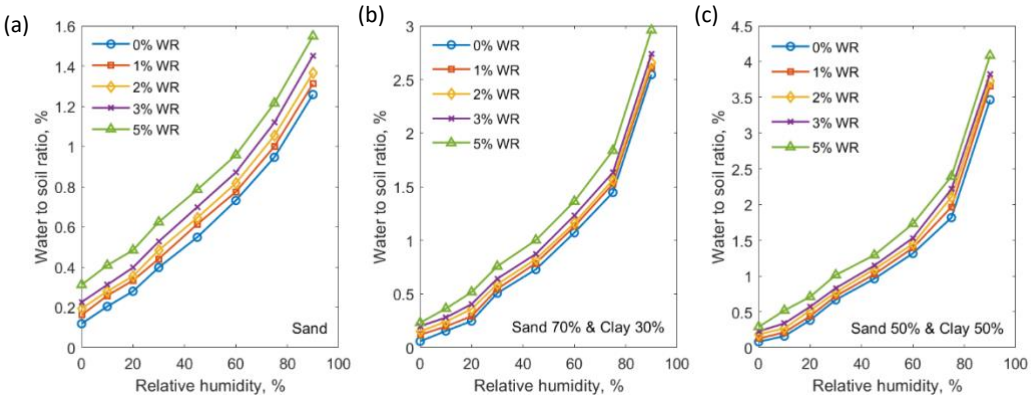

Figure 28: The measured water to dry soil weight ratio for different material, (a) sand, (b) 70 % sand and 30 % clay and (c) 50 % sand and 50 % clay.

The soil water diffusivity was measured by a 1D draining process, as shown in Figure 25(b). The containers of soil samples have open ends. The bottom of the soil samples was put on a dry filter paper. The water loss rate of soil samples was measured. The prepared soil samples had 4 different initial water contents, which were 14%, 16%, 18% and 20% by the weight of dry soil (w/s), and the pore water had 5 different water retainer concentration values, which were 0%, 1%, 3%, 5%, and 7%

by water volume. The 1D draining test was performed for two types of soil; they were sand and clayey sand (75% sand and 25% clay). Figure 29 shows the measured water loss rate (gram/second) for the samples of different initial water to dry soil ratio (w/s) and WR concentration (%). The results also demonstrate the beneficial effect of WR. Using the WR reduces the water loss rate of soils, particularly in high soil water content states.

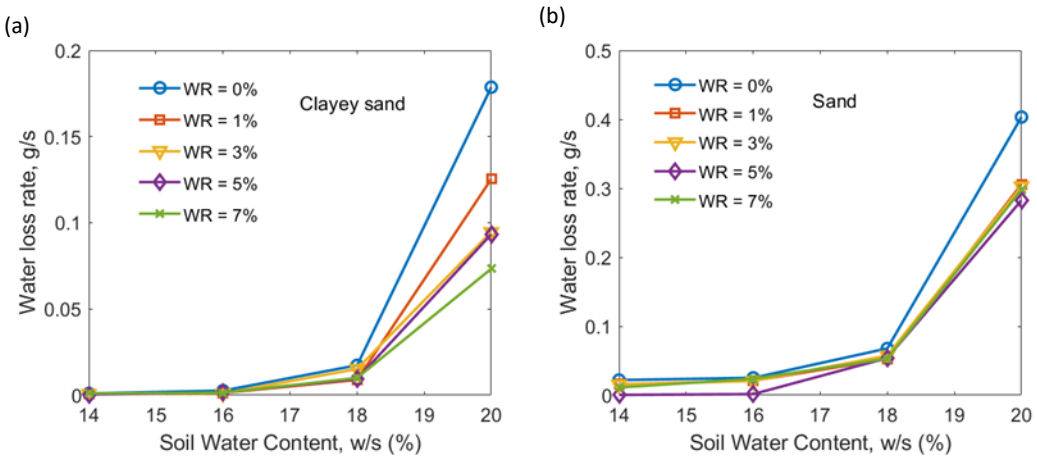

Figure 29: The measured water loss rate using 1-D draining test for (a) clayey sand and (b) sand.

II. Water Retention Curve Modelling

Soil water retention curves were worked out in terms of the measurements in Figure. 27 and Figure 28. However, from Figure 26, it can be seen that the current adopted relative control approach has less sensitivity or less accuracy for the low suction range. The curve of Figure 26 is almost flat when suction is less 1 MPa. So the current measurement is primarily to assess the water retainer effect at low water content or high suction range. The assessment primarily aims to assess the water retainer capacity to help reduce water evaporation under atmospheric conditions, as illustrated by the relative humidity map in Europe (Figure 30).

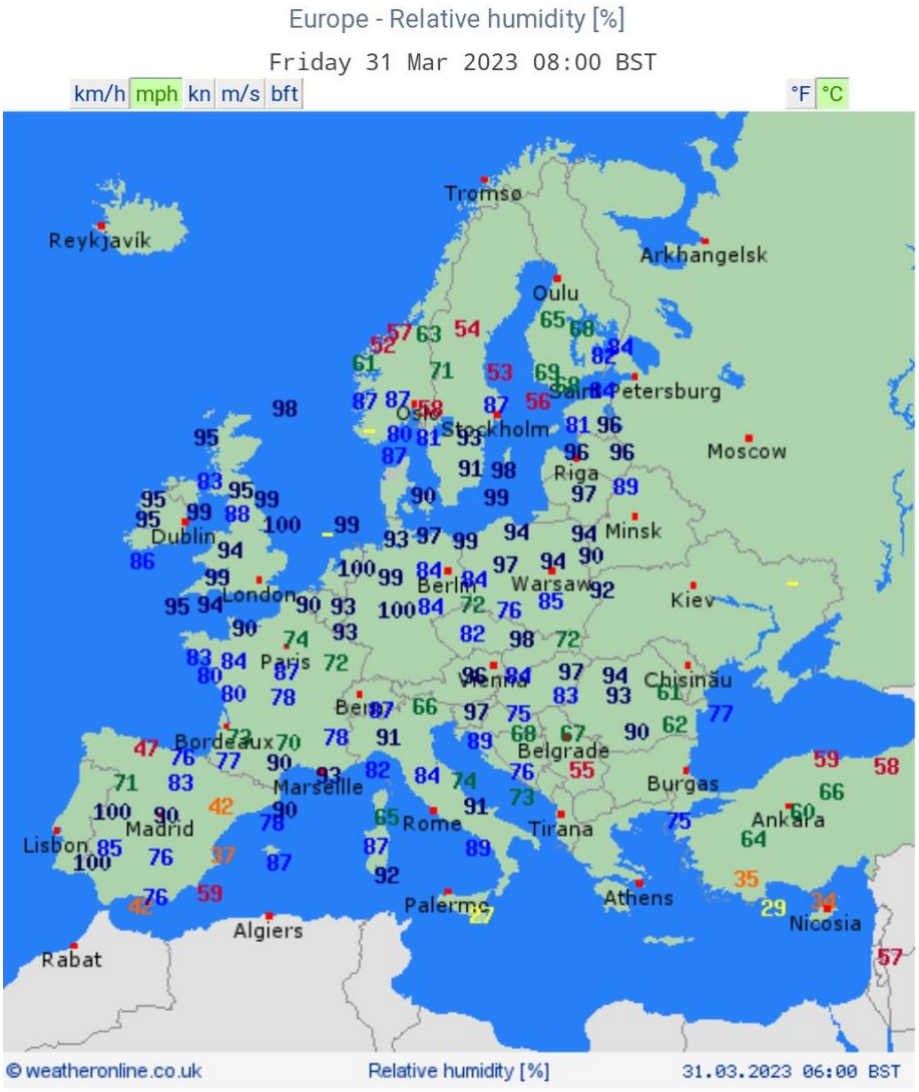

Figure 30: European atmospheric relative humidity states (https://www.weatheronline.co.uk/weather/maps/current?LANG=en&TYP=feuchte&ART=karte&CONT=euro&UP=0&R=310&CEL=C)

Two different models have been employed to characterize the effect of the water retainer on soil water retention curve change. The two models are:

- van Genuchten model (van Genuchten, M. Th. 1980. A closed-form equation for predicting the hydraulic conductivity of unsaturated soils. Soil, Sci. Soc. Am. J. 44:892-898.)

$$S_w = S_r + (S_s - S_r)\left[\frac{1}{1+(\alpha\psi_m)^n}\right]^{\left(1-\frac{1}{n}\right)}$$

where S_w is pore water saturation, S_r is residual pore water saturation, S_s is fully saturated pore water saturation, which takes account of the inaccessible pore spaces for water, such as that of trapped air or the pore range which the measuring approach cannot reach, such as pore space of free water; All

pore water saturation values are in the range between 0 and 1. ψ_m is matric suction (Pa); α (1/Pa) and n are two parametric constants.

Water Vapor Sorption – Water Retention Characteristic (WVS-WRC) model (1. Y. Wang, X.Y. Wang, M. Scholz, D.K. Ross, A physico-chemical model for the water vapour sorption isotherm of hardened cementitious materials, Construction and Building Materials 35 (2012) 941–946; 2. Vebleo - Scientific Conferences & Webinars - https://www.youtube.com/watch?v=tyYyK9TYdXQ)

$$\psi_m = \lambda\left[\frac{1}{\alpha}(\exp(\alpha S_w) - 1) - \frac{1}{\beta}(\exp(\beta(1 - S_w)) - 1)\right] + \chi(1 - S_w)^n$$

where λ (Pa), α, β, and χ (Pa) are four parametric constants; S_w is the pore water saturation in the range of 0~1.

4.6.2 First results

- Modelling of van Gunuchten model

Conventionally, soil water retention curves are presented as the relationship between the soil suction and soil pore water saturation degree. So, the first step needs express the measurement in Figure 28 as the pore water saturation, which was estimated to be the ratio of the soil water weight at unsaturated states to the soil water weight at fully saturated state. As it is hard to accurately determinate the just fully saturated state or pore water weight at the moment of relative humidity of 100%, the water saturation at just a fully saturated state was left to be determined by the modelling itself, for which the van-Guenchten model was rewritten as:

$$(w/s) = (w/s)_r + ((w/s)_s - (w/s)_r)\left[\frac{1}{1 + (\beta ln(RH))^n}\right]^{\left(1-\frac{1}{n}\right)}$$

where w/s is the water to soil ratio, the measurement of Figure 28; $\beta = -\alpha RT/V_w$ is a redefined parameter. At first, we used the above equation to fit the curves in Figure 28, and left the $(w/s)_s$ the maximum w/s or the determined fully saturated state to be determined by fitting performed. Thereafter, we use the determined (w/s)s to calculate the pore water saturation degree, i.e.: $S_w = \frac{(w/s)}{(w/s)_s}$. The worked water retention curves in term of water saturation were fitted again using the original van Genuchten formula (van Genuchten, 1980).

Fig. 31 displaces the water retention curve data worked out from Fig. 28 measurements following the calculation described above, and the modelling results using the van Genuchten model for the three types of soil. Table 6 lists the determined van Genuchten parameters for the represented water retention curves. The modelling results agree with the experimental data, which clearly show the effect of the water retainer on soil water retention capacity. At the same suction values, for all three soil types, the higher the water retainer concentration, the higher the pore water saturation in all the

measured suction ranges. It also can be noticed from the parameters in Table 6 that both the residual pore water saturation S_r and the maximum pore water saturation S_s increase with the concentration of the WR.

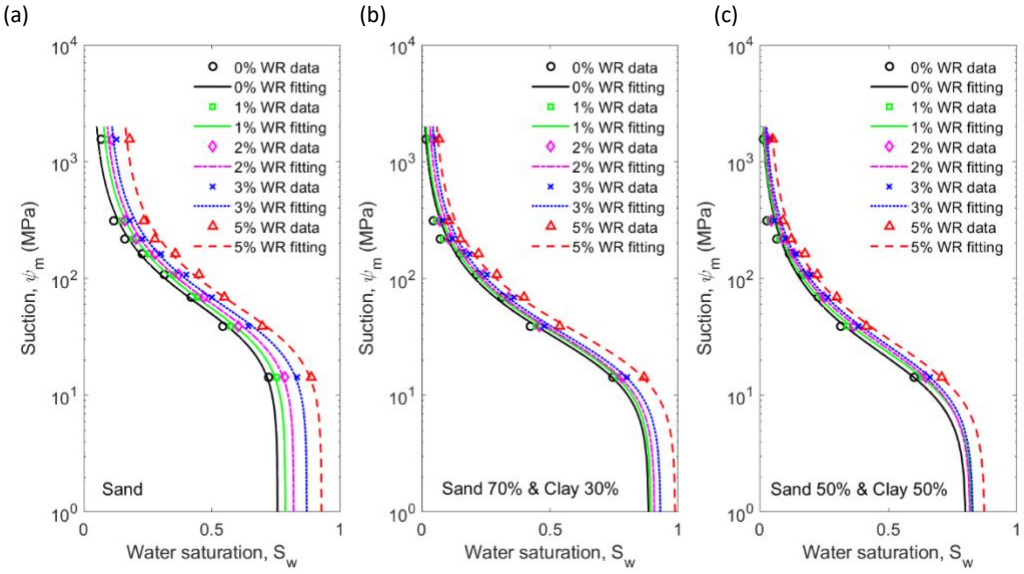

Figure 31: Modelled soil water retention curves according the van Genuchten model, for different soil textures and water retention concentrations, (a) 100 % sand, (b) 70 % sand and 30 % clay and (c) 50 % sand and 50 % clay.

Table 6: The fitted α, n, S_r and S_s parameters for the soil water retention curve of the Mualem-van Genuchten model.

Soil	WR content	α (1/MPa)	n	S_r	S_s
Sand	0%	0.02444	1.962	0.03378	0.7559
	1%	0.02432	1.962	0.06112	0.7861
	2%	0.02425	1.962	0.07448	0.8189
	3%	0.02455	1.962	0.09243	0.87
	5%	0.02479	1.962	0.1443	0.9272
Clayed sand A (70% sand & 30% clay)	0%	0.04598	1.936	1.38E-12	0.885
	1%	0.04342	1.936	0.004214	0.8938
	2%	0.04377	1.936	0.0179	0.9076
	3%	0.0434	1.936	0.02952	0.931
	5%	0.04073	1.936	0.04359	0.9887
Clayed sand B (50% sand & 50% clay)	0%	0.06559	1.863	2.19E-10	0.8022
	1%	0.06195	1.863	0.0001283	0.8268
	2%	0.05732	1.863	0.005406	0.8188
	3%	0.05538	1.863	0.01194	0.8297
	5%	0.05452	1.863	0.0321	0.8749

Figure 31 and Table 6 are the modelling results following the classic van Genuchten model. However, in hydrology practice, the parameter S_s is generally simplified to be 1 with no consider of the inaccessible pore space, for which the van Genuchten formulas is rewritten as:

$$S_w = S_r + (1 - S_r)\left[\frac{1}{1 + (\alpha\psi_m)^n}\right]^{\left(1-\frac{1}{n}\right)}$$

Figure 32 shows the results using the above equation to refit the data in Fig. 31. Table 7 list out the correspondingly determined parameters. It can be seen that modelling results still confirm the effect of the use of a water retainer, however, the simplified model itself presents a less accurate representation of the water retention curves.

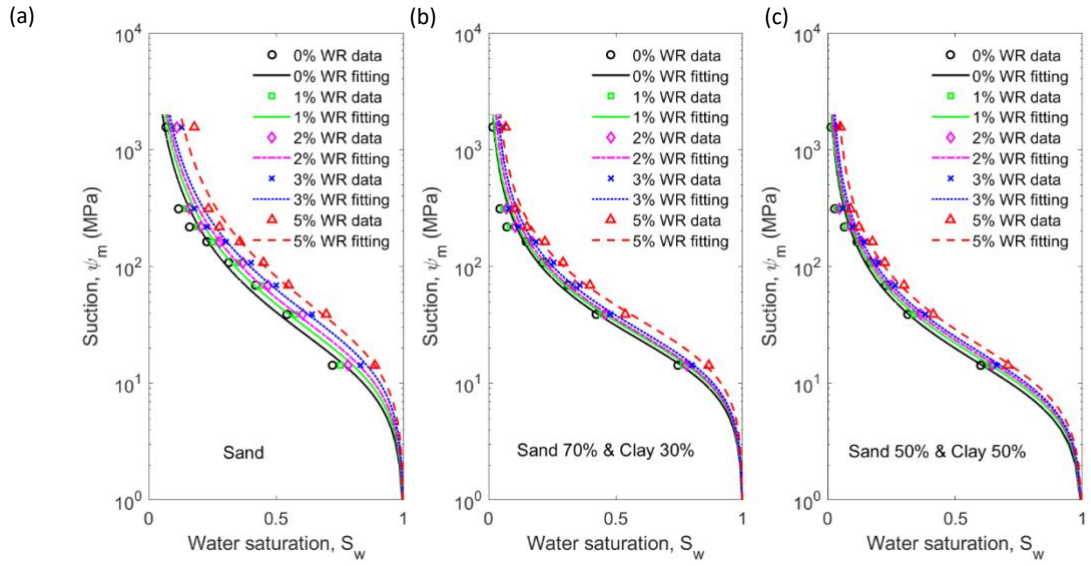

Figure 32: Modelled soil water retention curves according the simplified van Genuchten model (S_s = 1), for different soil textures and water retention concentrations, (a) 100 % sand, (b) 70 % sand and 30 % clay and (c) 50 % sand and 50 % clay.

Table 7: The fitted α, n, S_r and S_s parameters for the soil water retention curve of the simplified Mualem-van Genuchten model (S_s =1).

Soil	*WR content*	*α (1/MPa)*	*n*	*S_r*	*S_s*
Sand	*0%*	*0.07189*	*1.589*	*1.68E-08*	*1*
	1%	*0.06248*	*1.589*	*0.007667*	*1*
	2%	*0.05562*	*1.589*	*0.01192*	*1*
	3%	*0.04728*	*1.589*	*0.01431*	*1*
	5%	*0.04009*	*1.589*	*0.05336*	*1*
Clayed sand A (70% sand & 30% clay)	*0%*	*0.06377*	*1.841*	*3.01E-11*	*1*
	1%	*0.0586*	*1.841*	*8.27E-06*	*1*
	2%	*0.0571*	*1.841*	*0.01044*	*1*
	3%	*0.05371*	*1.841*	*0.0189*	*1*
	5%	*0.04425*	*1.841*	*0.02412*	*1*
Clayed sand B (50% sand & 50% clay)	*0%*	*0.1076*	*1.778*	*3.58E-07*	*1*
	1%	*0.09694*	*1.778*	*1.46E-06*	*1*
	2%	*0.09146*	*1.778*	*0.00389*	*1*
	3%	*0.08676*	*1.778*	*0.01032*	*1*
	5%	*0.07724*	*1.778*	*0.02654*	*1*

It has been deliberately set the van Genuchten parameter, n, unchanged with water retainer concentration, which takes the value of the benchmark curve, WR = 0% (no use of the water retainer). The reason to do this is based on the assumption that the water retainer has no relation to soil pore size distribution or pore structure. Figure 33(a) shows the variation of the other parameter, α, with the water retainer usage. Figure 33(b) shows the ratio of the α value to that of the benchmark (WR = 0%) at different WR concentrations for the data in Table 7.

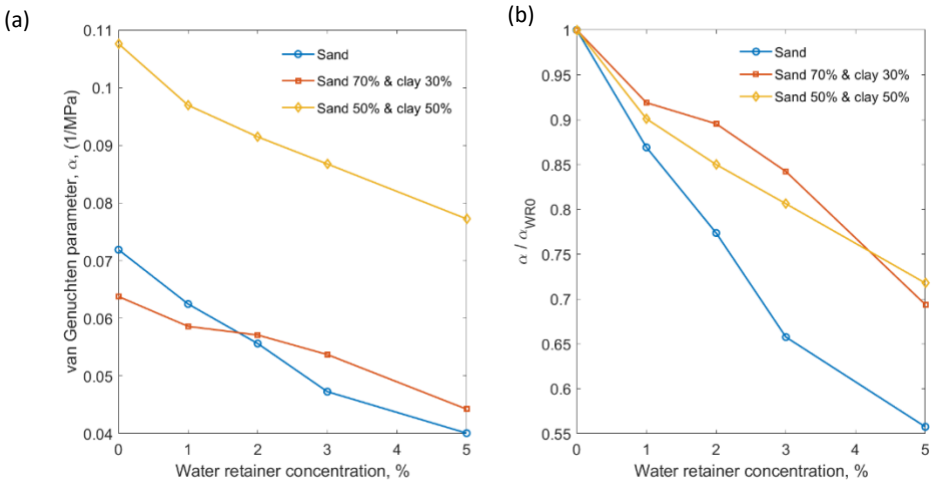

Figure 33: The variation of the van Genuchter parameter, α

- Modelling of VWS-WRC model

Figure 34 shows the modelling results using the WVS-WRC model for the saturation range starting from the saturated state defined by Figure 27(a). The data and modelling results demonstrates that the water retainer effect is more pronounced at low soil water content.

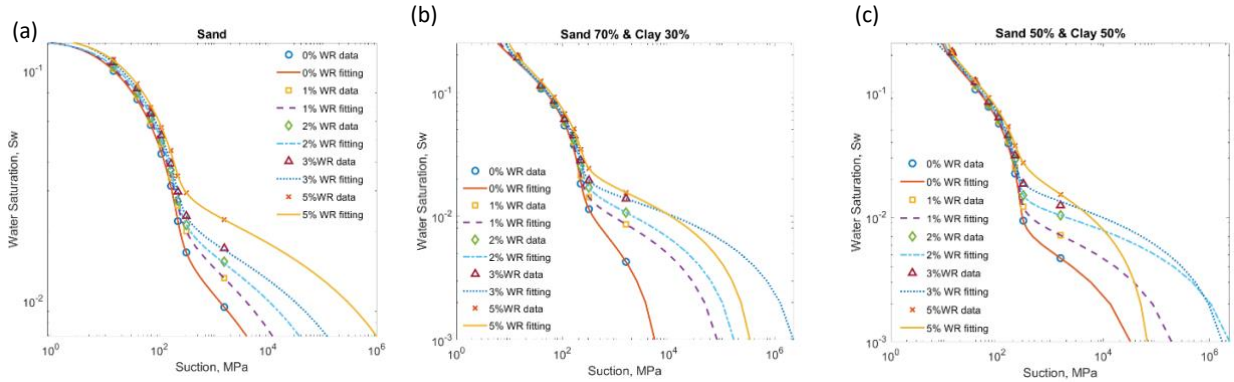

Figure 34: Modelled soil water retention curves according the WVS-WRC model, for different soil textures and water retention concentrations, (a) 100 % sand, (b) 70 % sand and 30 % clay and (c) 50 % sand and 50 % clay.

Table 8 lists out the obtained parameter values for the modelling results in Figure 34.

Table 8: The fitted parameters for the soil water retention curve of the WVS-WRC model.

Soil sample	Porosity	WVS-WRC Parameter	WR 0%	WR 1%	WR 2%	WR 3%	WR 5%
Sand	0.26	A	–30.06	–30.15	–28.88	–29.25	–28.96
Clayey sand A	0.28		–19.24	–19.58	–21.48	–21.5	–21.71
Clayey sand B	0.35		–21.96	–22.25	–21.83	–19.24	–22.92
Sand	0.26	B	–30.56	–30.66	–29.48	–29.72	–29.48
Clayey sand A	0.28		–19.02	–19.33	–21.1	–21.14	–21.34
Clayey sand B	0.35		–21.47	–21.69	–21.35	–19.01	–22.44
Sand	0.26	Λ	–1.31E+4	–1.45E+4	–1.43E+4	–1.57E+4	–1.80E+4
Clayey sand A	0.28		–5920	–6411	–7940	–8418	–9769
Clayey sand B	0.35		–7687	–8224	–8472	–7077	–1.13E+4
Sand	0.26	χ	9.27E+4	2.01E+5	8.67E+5	3.37E+6	1.98E+7
Clayey sand A	0.28		7794	1.39E+5	2.76E+5	3.95E+6	4.92E+5
Clayey sand B	0.35		7.69E+4	4.32E+5	5.32E+6	3.07E+6	8.79E+4
Sand	0.26	N	4.58E+2	4.04E+2	4.47E+2	4.72E+2	4.25E+2
Clayey sand A	0.28		422.4	5.43E+2	5.01E+2	5.77E+2	3.83E+2
Clayey sand B	0.35		8.78E+2	8.14E+2	8.05E+2	5.79E+2	2.79E+2

The analysis, interpretation, modelling and characterization for the 1D draining test measurement data are still undergoing.

5 Discussion on the usability of solutions/models for stakeholder

The solutions developed in WATERAGRI are intended to support decision-making in agriculture. As presented in this report, numerical models solving physical equations are a suitable tool to provide information on, for example, the evolution of soil moisture or water levels in channels as a function of time, considering local conditions, water, climate and climate and land use scenarios. Despite sparse data availability, large-scale numerical models have been developed in Finland and Poland that can simulate broadly general trends in groundwater levels or soil moisture. Compared to existing tools, these models already appear to be useful for simulating the impact of weather variability on agricultural activities. Further model improvement, e.g., a realistic consideration of hydraulic conditions (including more appropriate boundary conditions), as well as the inclusion of local measurements in either a classical calibration routine, a pilot point approach, or a data assimilation step is planned and promises more reliable model results for stakeholders. Soil hydraulic properties determined in the laboratory (USAL) can include the impact of the water retainer on the modification of the soil hydraulic properties and be used to modify the water retention and relative permeability curves for the different soil textures present in an area where the water retainer was applied. It allows

us to better simulate the water retainer's impact on soil hydrology. Alternatively, stakeholders involved in the project can help improve the models by bringing in their on-site observations.

A real-time modelling framework (A1) was developed and is presented in this report, integrating field data, modelling approaches, and weather forecasts. The results are partially available online at the time of writing this report, and further online visualization is underway. In addition, developments for the German case study site are replicated for the Hungarian site to mimic and investigate to which extent a numerical model (CLM) could update irrigation rates in near-real time.

Overall, WATERAGRI developments are already at the stage where operational simulations can be performed that allows real-time assessment. For example, active management of the surrounding channels (i.e., considering the model data) at the Seeland site in Switzerland can significantly reduce the soil water deficit. To verify if the model developments are going in the right direction, UNINE organized a small-scale workshop with local stakeholders on January 13, 2023, in Seeland, Switzerland. This workshop was conducted jointly with the largest farmers' association in the Seeland - Grosses Moos region and the local engineering company RSW AG. The strategies and objectives of the WATERAGRI project were presented, and the results of modelling simulations with the new drainage system were presented and discussed. Suggestions for further improvement of the model configuration in Seeland and partly for other sites were made and implemented.

Therefore, WATERAGRI's solutions are always actively discussed with stakeholders to improve our models in the desired direction. The largest stakeholder workshop was WATERGARI Workshop #3, which gave us a clear idea of what information the models should provide for near real-time agricultural decision-making. Participating stakeholders requested site-specific modelling and wanted model results that could be made available online and on smartphones in charts, tables, and figures.

This and feedback gathered in other stakeholder discussions make it clear that the real-time modelling framework developed meets stakeholder expectations. This is fundamental for the data assimilation framework (A2) that will provide optimal estimates of soil, crop, and water conditions, which in turn will contribute to precision irrigation and optimization of irrigation schedules days in advance and reduce potential costs to farmers (e.g., for disproportionate irrigation).

6 Conclusion and Outlook

This report presents the assessment of WATERAGRI solutions at the case study sites in Germany, Switzerland, Poland, Hungary and Finland. At all sites', physically based models are being developed either with HydroGeoSphere or the Terrestrial System Modelling Platform. The models in their current version build the real-time modelling framework of WATERAGRI (A1). All models can integrate site-specific soil and meteorological data and weather forecasts. For example, large-scale models for Finland and Poland provide an initial assessment of general trends in hydraulic heads and soil moisture, contributing to an initial understanding of the impact of weather variability on local agricultural watersheds. Replication at the Hungarian site provides an initial assessment of how on-site measurements combined with a physically-based model could allow near real-time optimization of irrigation schedules, minimizing irrigation water waste.

Similarly, the models developed in Switzerland and Germany allow agricultural decision-making to be mimicked at the plot level, which in turn allows further exploration of their usability by stakeholders. For example, the model developed by UNINE allows for improved management of surrounding canals resulting in reduced soil water deficits, and the model by FZJ provides a new 10-day soil moisture forecast every day. Both were presented and discussed with local stakeholders.

In parallel, some first development runs for the data assimilation framework (A2) could be performed using the models developed for the case study sites in Germany and Switzerland. For example, the performance of the developed data assimilation system for the case study site in Switzerland has been tested with a synthetic alluvial plain model set up by (Delottier et al., 2022). The data assimilation results show that the model states are reasonably well-constrained during the pumping period. It will be extended later and tested for the Seeland model.

This option can be considered in the data assimilation framework (A2) that is designed to provide the best possible initial condition for a forecast model and predicts hydrological and crop states for the next two weeks with reduced uncertainty, i.e., that can provide operational site-specific soil moisture ensemble forecasts. Simulation experiments at the WATERARGI case study sites with and without weather forecasts and with and without data assimilation as well as the potential use for stakeholders, are part of D7.5 and ongoing at the time of this report.

7 References

Aalto, J., Pirinen, P., & Jylhä, K. (2016). New gridded daily climatology of Finland: Permutation-based uncertainty estimates and temporal trends in climate. *Journal of Geophysical Research: Atmospheres*, *121*(8), 3807–3823. https://doi.org/10.1002/2015JD024651

Ala-aho, P., Soulsby, C., Wang, H., & Tetzlaff, D. (2017). Integrated surface-subsurface model to investigate the role of groundwater in headwater catchment runoff generation: A minimalist approach to parameterisation. *Journal of Hydrology*, *547*, 664–677. https://doi.org/10.1016/j.jhydrol.2017.02.023

Aquanty, I. (2020). *HydroGeoSphere: A three-dimensional numerical model describing fully-integrated subsurface and surface flow and solute transport*. Waterloo: Aquanty Inc.

Ashby, S. F., & Falgout, R. D. (1996). A Parallel Multigrid Preconditioned Conjugate Gradient Algorithm for Groundwater Flow Simulations. *Nuclear Science and Engineering*, *124*(1), 145–159. https://doi.org/10.13182/NSE96-A24230

Baldauf, M., Seifert, A., Förstner, J., Majewski, D., Raschendorfer, M., & Reinhardt, T. (2011). Operational Convective-Scale Numerical Weather Prediction with the COSMO Model: Description and Sensitivities. *Monthly Weather Review*, *139*(12), 3887–3905. https://doi.org/10.1175/MWR-D-10-05013.1

Boas, T., Bogena, H., Grünwald, T., Heinesch, B., Ryu, D., Schmidt, M., Vereecken, H., Western, A., & Hendricks Franssen, H.-J. (2021). Improving the representation of cropland sites in the Community Land Model (CLM) version 5.0. *Geoscientific Model Development*, *14*(1), 573–601. https://doi.org/10.5194/gmd-14-573-2021

Bogena, H. R., Montzka, C., Huisman, J. A., Graf, A., Schmidt, M., Stockinger, M., Hebel, C. von, Hendricks-Franssen, H. J., van der Kruk, J., Tappe, W., Lücke, A., Baatz, R., Bol, R., Groh, J., Pütz, T.,

Jakobi, J., Kunkel, R., Sorg, J., & Vereecken, H. (2018). The TERENO-Rur Hydrological Observatory: A Multiscale Multi-Compartment Research Platform for the Advancement of Hydrological Science. *Vadose Zone Journal*, *17*(1), 180055. https://doi.org/10.2136/vzj2018.03.0055

Bonton, A., Bouchard, C., Rouleau, A., Rodriguez, M. J., & Therrien, R. (2012). Calibration and validation of an integrated nitrate transport model within a well capture zone. *Journal of Contaminant Hydrology*, *128*(1-4), 1–18. https://doi.org/10.1016/j.jconhyd.2011.10.007

Brunner, P., & Simmons, C. T. (2012). HydroGeoSphere: A Fully Integrated, Physically Based Hydrological Model. *Ground Water*, *50*(2), 170–176. https://doi.org/10.1111/j.1745-6584.2011.00882.x

Burgers, G., van Jan Leeuwen, P., & Evensen, G. (1998). Analysis Scheme in the Ensemble Kalman Filter. *Monthly Weather Review*, *126*(6), 1719–1724. https://doi.org/10.1175/1520-0493(1998)126<1719:ASITEK>2.0.CO;2

Chow, V. T. (1959). *Open Channel Hydraulics*. New York: McGraw-Hill.

Davison, J. H., Hwang, H.-T., Sudicky, E. A., & Lin, J. C. (2015). Coupled atmospheric, land surface, and subsurface modelling: Exploring water and energy feedbacks in three-dimensions. *Advances in Water Resources*, *86*, 73–85. https://doi.org/10.1016/j.advwatres.2015.09.002

Delottier, H., Peel, M., Musy, S., Schilling, O. S., Purtschert, R., & Brunner, P. (2022). Explicit simulation of environmental gas tracers with integrated surface and subsurface hydrological models. *Frontiers in Water*, *4.* https://doi.org/10.3389/frwa.2022.980030

Doherty, J. (2010). *PEST: Model-Independent Parameter Estimation*. Abstract.

Downer, C.W. and Ogden, F.L. (2004) Appropriate Vertical Discretization of Richards' Equation for Two-Dimensional Watershed-Scale Modelling. Hydrological Processes, 18, 1-22. http://dx.doi.org/10.1002/hyp.1306

Feddes, R. A., Kowalik, P. J., & Zaradny, H. (1978). *Simulation of field water use and crop yield*. Simulation monographs. New York: Wiley.

Feddes, R. A., Rooij, G. H. de, & van Dam, J. C. (Eds.). (2004). Wageningen UR frontis series: *volume 6*. *Unsaturated-zone modelling: Progress, challenges and applications*. Dordrecht: Kluwer academic Publishers.

Fiers, M., Edel-Hermann, V., Chatot, C., Le Hingrat, Y., Alabouvette, C., & Steinberg, C. (2012). Potato soil-borne diseases. A review. *Agronomy for Sustainable Development*, *32*(1), 93–132. https://doi.org/10.1007/s13593-011-0035-z

Fredlund, Delwyn. (1989). Soil Suction Monitoring For Roads and Airfields. SYMPOSIUM State-of-the-Art of Pavement Response Monitoring Systems for Roads and AirfieldsAt: West Lebanon New Hampshire USA

Gasper, F., Goergen, K., Shrestha, P., Sulis, M., Rihani, J., Geimer, M., & Kollet, S. (2014). Implementation and scaling of the fully coupled Terrestrial Systems Modeling Platform (TerrSysMP v1.0) in a massively parallel supercomputing environment – a case study on JUQUEEN (IBM Blue Gene/Q). *Geoscientific Model Development*, *7*(5), 2531–2543. https://doi.org/10.5194/gmd-7-2531-2014

Geological Survey of Finland. (2017). *Stratum data for superficial deposits [database]*. Abstract.

Johansson, P., Räisänen, J., & Väisänen, U. (2005). *Superficial deposits of Tyrnävä area, Superficial deposits 1:20 000 interpretation* (No. sheet 342106 [In Finnish]).

Kennedy, D., Swenson, S., Oleson, K. W., Lawrence, D. M., Fisher, R., Da Lola Costa, A. C., & Gentine, P. (2019). Implementing Plant Hydraulics in the Community Land Model, Version 5. *Journal of Advances in Modeling Earth Systems*, *11*(2), 485–513. https://doi.org/10.1029/2018MS001500

Kollet, S. J., & Maxwell, R. M. (2006). Integrated surface–groundwater flow modeling: A free-surface overland flow boundary condition in a parallel groundwater flow model. *Advances in Water Resources*, *29*(7), 945–958. https://doi.org/10.1016/j.advwatres.2005.08.006

Kristensen, K. J., & Jensen, S. E. (1975). A model for estimating actual evapotranspiration from potential evapotranspiration. *Hydrology Research*, *6*(3), 170–188. https://doi.org/10.2166/nh.1975.0012

Kurtz, W., He, G., Kollet, S. J., Maxwell, R. M., Vereecken, H., & Hendricks Franssen, H.-J. (2016). TerrSysMP–PDAF (version 1.0): a modular high-performance data assimilation framework for an integrated land surface–subsurface model. *Geoscientific Model Development*, *9*(4), 1341–1360. https://doi.org/10.5194/gmd-9-1341-2016

Kurtz, W., Lapin, A., Schilling, O. S., Tang, Q., Schiller, E., Braun, T., Hunkeler, D., Vereecken, H., Sudicky, E., Kropf, P., Hendricks Franssen, H.-J., & Brunner, P. (2017). Integrating hydrological modelling, data assimilation and cloud computing for real-time management of water resources. *Environmental Modelling & Software*, *93*, 418–435. https://doi.org/10.1016/j.envsoft.2017.03.011

Lawrence, D. M., Fisher, R. A., Koven, C. D., Oleson, K. W., Swenson, S. C., Bonan, G., Collier, N., Ghimire, B., Kampenhout, L., Kennedy, D., Kluzek, E., Lawrence, P. J., Li, F., Li, H., Lombardozzi, D., Riley, W. J., Sacks, W. J., Shi, M., Vertenstein, M., Wieder, W. R., Xu, C., Ali, A. A., Badger, A. M., Bisht, G., Broeke, M., Brunke, M. A., Burns, S. P., Buzan, J., Clark, M., Craig, A., Dahlin, K., Drewniak, B., Fisher, J. B., Flanner, M., Fox, A. M., Gentine, P., Hoffman, F., Keppel-Aleks, G., Knox, R., Kumar, S., Lenaerts, J., Leung, L. R., Lipscomb, W. H., Lu, Y., Pandey, A., Pelletier, J. D., Perket, J., Randerson, J. T., Ricciuto, D. M., Sanderson, B. M., Slater, A., Subin, Z. M., Tang, J., Thomas, R. Q., Val Martin, M., & Zeng, X. (2019). The Community Land Model Version 5: Description of New Features, Benchmarking, and Impact of Forcing Uncertainty. *Journal of Advances in Modeling Earth Systems*, *11*(12), 4245–4287. https://doi.org/10.1029/2018MS001583

Liedes, T., Pylvänäinen, J., Torvela, J., Aurio, V., Tuula, L., Sakari, N., & Esa, T. (2020). *Final report of the TIMAKO project on the data driven soil moisture control*. Abstract.

Liggett, J. E., Werner, A. D., & Simmons, C. T. (2012). Influence of the first-order exchange coefficient on simulation of coupled surface–subsurface flow. *Journal of Hydrology*, *414-415*, 503–515. https://doi.org/10.1016/j.jhydrol.2011.11.028

Maaseutunverkosto. (2009). *Controlled drainage [brochure, In Finnish]*. Abstract.

Martin, R. J., Jamieson, P. D., Wilson, D. R., & Francis, G. S. (1992). Effects of soil moisture deficits on yield and quality of 'Russet Burbank' potatoes. *New Zealand Journal of Crop and Horticultural Science*, *20*(1), 1–9. https://doi.org/10.1080/01140671.1992.10422319

Maxwell, R. M. (2013). A terrain-following grid transform and preconditioner for parallel, large-scale, integrated hydrologic modeling. *Advances in Water Resources*, *53*, 109–117. https://doi.org/10.1016/j.advwatres.2012.10.001

National Land Survey of Finland. (2023). *Elevation model 2008-2020, 2 m x 2 m*. Abstract.

Nerger, L., & Hiller, W. (2013). Software for ensemble-based data assimilation systems—Implementation strategies and scalability. *Computers & Geosciences*, *55*, 110–118. https://doi.org/10.1016/j.cageo.2012.03.026

Oleson, K. W., Niu, G.-Y., Yang, Z.-L., Lawrence, D. M., Thornton, P. E., Lawrence, P. J., Stöckli, R., Dickinson, R. E., Bonan, G. B., Levis, S., Dai, A., & Qian, T. (2008). Improvements to the Community Land Model and their impact on the hydrological cycle. *Journal of Geophysical Research: Biogeosciences*, *113*(G1), n/a-n/a. https://doi.org/10.1029/2007JG000563

Panday, S., & Huyakorn, P. S. (2004). A fully coupled physically-based spatially-distributed model for evaluating surface/subsurface flow. *Advances in Water Resources*, *27*(4), 361–382. https://doi.org/10.1016/j.advwatres.2004.02.016

Pirinen, P., Lehtonen, I., Heikkinen, R. K., Aapala, K., & Aalto, J. (2022). FMI's Climate Bulletin Research Letters 2/2022. *Ilmastokatsaus*, *4*(2), 35–37. https://doi.org/10.35614/ISSN-2341-6408-IK-2022-11-RL

Pulido-Bosch, A., Rigol-Sanchez, J. P., Vallejos, A., Andreu, J. M., Ceron, J. C., Molina-Sanchez, L., & Sola, F. (2018). Impacts of agricultural irrigation on groundwater salinity. *Environmental Earth Sciences*, *77*(5). https://doi.org/10.1007/s12665-018-7386-6

Reichle, R. H. (2008). Data assimilation methods in the Earth sciences. *Advances in Water Resources*, *31*(11), 1411–1418. https://doi.org/10.1016/j.advwatres.2008.01.001

Rintanen, S. (1985). Measurements of hydraulic conductivity, its spatial variability and use designing subsurface land drainage [In Finnish] (Master's thesis). Helsinki University of TechnologyHelsinki,

Rooij, R. de. (2017). *A consistent implementation of the dual node approach for coupling surface-subsurface flow and its comparison to the common node approach*. Abstract.

Schepper, G. de, Therrien, R., Refsgaard, J. C., He, X., Kjaergaard, C., & Iversen, B. V. (2017). Simulating seasonal variations of tile drainage discharge in an agricultural catchment. *Water Resources Research*, *53*(5), 3896–3920. https://doi.org/10.1002/2016WR020209

Schilling, O. S., Doherty, J., Kinzelbach, W., Wang, H., Yang, P. N., & Brunner, P. (2014). Using tree ring data as a proxy for transpiration to reduce predictive uncertainty of a model simulating groundwater–surface water–vegetation interactions. *Journal of Hydrology*, *519*, 2258–2271. https://doi.org/10.1016/j.jhydrol.2014.08.063

Schilling, O. S., Irvine, D. J., Hendricks Franssen, H.-J., & Brunner, P. (2017). Estimating the Spatial Extent of Unsaturated Zones in Heterogeneous River-Aquifer Systems. *Water Resources Research*, *53*(12), 10583–10602. https://doi.org/10.1002/2017WR020409

Schilling, O. S., Park, Y.-J., Therrien, R., & Nagare, R. M. (2019). Integrated Surface and Subsurface Hydrological Modeling with Snowmelt and Pore Water Freeze-Thaw. *Groundwater*, *57*(1), 63–74. https://doi.org/10.1111/gwat.12841

Shrestha, P., Sulis, M., Masbou, M., Kollet, S., & Simmer, C. (2014). A Scale-Consistent Terrestrial Systems Modeling Platform Based on COSMO, CLM, and ParFlow. *Monthly Weather Review*, *142*(9), 3466–3483. https://doi.org/10.1175/MWR-D-14-00029.1

Strebel, L., Bogena, H. R., Vereecken, H., & Hendricks Franssen, H.-J. (2022). Coupling the Community Land Model version 5.0 to the parallel data assimilation framework PDAF: description and applications. *Geoscientific Model Development*, *15*(2), 395–411. https://doi.org/10.5194/gmd-15-395-2022

Swenson, S. C., Clark, M., Fan, Y., Lawrence, D. M., & Perket, J. (2019). Representing Intrahillslope Lateral Subsurface Flow in the Community Land Model. *Journal of Advances in Modeling Earth Systems*, *11*(12), 4044–4065. https://doi.org/10.1029/2019MS001833

Tang, Q., Kurtz, W., Schilling, O. S., Brunner, P., Vereecken, H., & Hendricks Franssen, H.-J. (2017). The influence of riverbed heterogeneity patterns on river-aquifer exchange fluxes under different connection regimes. *Journal of Hydrology*, *554*, 383–396. https://doi.org/10.1016/j.jhydrol.2017.09.031

Tang, Q., Schilling, O. S., Kurtz, W., Brunner, P., Vereecken, H., & Hendricks Franssen, H.-J. (2018). Simulating Flood-Induced Riverbed Transience Using Unmanned Aerial Vehicles, Physically Based Hydrological Modeling, and the Ensemble Kalman Filter. *Water Resources Research*, *54*(11), 9342–9363. https://doi.org/10.1029/2018WR023067

Valcke, S. (2013). The OASIS3 coupler: a European climate modelling community software. *Geoscientific Model Development*, *6*(2), 373–388. https://doi.org/10.5194/gmd-6-373-2013

van Genuchten, M. T. (1980). A Closed-form Equation for Predicting the Hydraulic Conductivity of Unsaturated Soils. *Soil Science Society of America Journal*, *44*(5), 892–898. https://doi.org/10.2136/sssaj1980.03615995004400050002x

Wang, Y., Wang, X.Y., Scholz, M. & Ross, D.K. (2012). A physico-chemical model for the water vapour sorption isotherm of hardened cementitious materials. *Construction and Building Materials, 35*, 941–946; - (Vebleo - Scientific Conferences & Webinars - https://www.youtube.com/watch?v=tyYyK9TYdXQ)